Isothermal and dynamic oxidation behaviour of Mo−W doped carbon-based coating

MANDAL, Paranjayee, EHIASARIAN, Arutiun <http://orcid.org/0000-0001-6080-3946> and HOVSEPIAN, Papken <http://orcid.org/0000-0002-1047-0407>

Published version

Repository use policy

Isothermal and dynamic oxidation behaviour of Mo − W doped carbon-based coating

Paranjayee Mandal*, Arutiun P. Ehiasarian and Papken Eh. Hovsepian

Nanotechnology Centre for PVD Research, HIPIMS Research Centre, Sheffield Hallam University, City Campus, Howard Street, Sheffield S1 1WB, United Kingdom

Email: 200712mum@gmail.com*, a.ehiasarian@shu.ac.uk, p.hovsepian@shu.ac.uk

Abstract

The oxidation behaviour of Mo−W doped carbon-based coating (Mo−W−C) is investigated in elevated temperature (400°C−1000°C). Strong metallurgical bond between Mo−W−C coating and substrate prevents any sort of delamination during heat-treatment. Isothermal oxidation tests show initial growth of metal oxides at 500°C, however graphitic nature of the as-deposited coating is preserved. The oxidation progresses with further rise in temperature and the substrate is eventually exposed at 700°C. The performance of Mo−W−C coating is compared with a state-of-the-art $DLC(Cr/Cr-WC/W:C-H/a:C-H)$ coating, which shows preliminary oxidation at 400°C and local delamination of the coating at 500°C leading to substrate exposure. The graphitisation starts at 400°C and the diamond-like structure is completely converted into the graphite-like structure at 500°C. Dynamic oxidation behaviour of both the coatings is investigated using Thermo-gravimetric analysis carried out with a slow heating rate of 1°C/min from ambient temperature to 1000°C. Mo−W−C coating resists oxidation up to ~800°C whereas delamination of $DLC(Cr/Cr-WC/W:C-H/a:C-H)$ coating is observed beyond ~380°C. In summary, Mo−W−C coating provides improved oxidation resistance at elevated temperature compared to $DLC(Cr/Cr-WC/W:C-H/a:C-H)$ coating.

Keywords: Oxidation, TGA, XRD, Raman spectroscopy

1. Introduction

Tribological applications of standard diamond-like-carbon (DLC) coatings in automotive industry are often compromised due to degradation of the coating properties at higher working temperature (>300°C). Significant amount of sp^3 bonded carbon present in the DLC coating results in diamond-like structure, which is found stable up to ~300°C. As the temperature reaches to ~350°C, the sp^3 bonded carbon is converted into sp^2 bonded carbon indicating initiation of graphitisation (i.e. transformation of diamond-like structure into graphite-like structure) and further rise in temperature results in complete graphitisation of the DLC coating. Raman spectroscopy is a popular non-destructive technique to study the bonding properties of the DLC coating. Raman frequencies of sp^3 and sp^2 sites in the crystalline diamond and graphite are found ~1330 cm^{-1} and ~1550 cm^{-1} respectively, thus this technique shows a notable distinction between sp^3 and sp^2 bonded carbon present in the DLC coating. The Raman spectrum of DLC coating is dominated by the G (sp^2 bonded graphitic carbon) peak from ambient condition to 300°C and a D (disordered) peak is appeared in the spectrum ~350°C showing start of graphitisation. The distinct and dominant D and G peaks are observed in the spectrum at ~450°C indicating complete transformation of the DLC coating into nanocrystalline graphite [1]. The nanocrystalline graphite does not possess the superior mechanical and tribological characteristics of the DLC coating leading to its failure at elevated temperature. In brief, the transformation of diamond-like structure into the graphite-like structure at ~350°C degrades the properties of DLC coating [1 − 3]. Incorporation of dopants like Ti, Si, Cr, Mo or W delays the graphitisation process and thus increases the thermal stability [2 − 10] as explained in the following paragraphs.

A recent study used electron cyclotron resonance chemical vapour deposition (ECR-CVD) with magnetron sputtering to deposit the Ti-DLC coating, which was found thermally stable

up to ~450°C after annealing of 30 minutes at ambient condition [2]. The formation of hard TiC phases during heat-treatment delayed the graphitisation of the coating. In another study, a multilayer Ti-DLC coating ($Ti/TiN/TiC_xN_y/DLC$) was deposited using combined UBM and PECVD techniques and thermal stability of this coating was tested by thermo-gravimetric analyser (TGA) with a heating rate of 15°C/min from room temperature to 800°C. The top DLC layer was graphitised below 350°C leading to a sudden decrease in hardness of the coating. In the temperature range 350°C − 450°C, a rapid weight loss was occurred due to formation of CO_2. Thus the Ti-containing intermediate layers were exposed and formation of TiO_2 led to gradual increase in the sample weight after 450°C [3]. When DLC coating was doped with both Ti and Al [nc-TiC/a-C(Al)] and deposited using UBM, a significant structural modification took place after 400°C as indicated by the sudden rise in the I_D/I_G ratio. The amorphous carbon matrix became almost graphite-like with a large cluster size as the temperature reached to 500°C. However, the presence of hard TiC phases retained the coating hardness almost similar even after the structural change [4].

Further research was carried out on the mid-frequency magnetron sputtered Si-DLC films, which was thermally stable up to 500°C after 30 minutes of annealing at ambient air [5]. The formation of silicon oxide was considered as a key factor to prevent diffusion of oxygen into the DLC coating. Another study reported that the graphitisation of RF sputtered Si-DLC film was started at ~400°C and significant oxidation was observed at ~500°C when annealing was done for 1 hour at ambient air [6]. The change in coating structure was confirmed by the rapid increase in the I_D/I_G ratio at ~500°C. The addition of Si stabilised the coating structure by forming more sp^3 bonded carbon, thus the graphitisation was delayed. Similar thermal stability was documented for conventional RF sputtered a-$C_{1-x}Si_x$:H coating in another

3

research [7]. The graphitisation took place ~500°C for samples with silicon content less than 15%. When silicon content was more than 15%, the structural change was delayed.

The thermal stability of Cr-DLC coating deposited using CAE technique was investigated using TGA with a heating rate of 10°C/min in the temperature range of 25˚C – 800°C [8]. The graphitisation started below 290°C and a significant weight loss was observed due to CO_2 formation in between 290˚C – 342°C. The oxidation of CrN and CrC_xN_y interlayers led to weight gain in the temperature range of 400˚C – 800°C. The annealing tests were carried out in the range of 200°C – 500°C for 30 minutes. The graphitisation started only at 200˚C and the groove formation was observed on the surface indicating the relaxation of internal residual stresses at 300°C. In another study, thermal stability of ~400˚C was reported for Cr-doped graphite-like carbon coating (C/Cr), which was deposited using combined steered cathodic arc and unbalanced magnetron sputtering [9]. The TGA analysis carried out with a heating rate of 1°C/min demonstrated two stages of oxidation at ~400˚C and ~660˚C respectively. The first stage of oxidation at ~400˚C was indicated by the weight loss due to rapid evaporation of carbon and the second stage at ~660˚C was indicated by the weight gain due to chromium oxide formation. Annealing tests were carried out for 1 hour in the temperature range 350˚C – 700°C. Depending on the bias voltages used during deposition of the C/Cr coatings, the oxidation took place in the temperature range of 410˚C – 700°C.

The thermal stability of Mo-DLC and W-DLC coatings deposited using filtered metal cathodic arc vacuum discharge technique were investigated in the temperature range of 200˚C – 500°C in Argon atmosphere. The Raman spectroscopy showed that the D and G peaks were disappeared at 400°C for DLC coating but they were present up to ~500°C for both the Mo-DLC and W-DLC coatings. The slower graphitisation rate of Mo-DLC and W-DLC coatings

was attributed to the presence of metal carbide phases, which were thermally stable and continued to coalesce below 500°C [10]. It can be summarised that the thermal stability of the metal-doped DLC coating strongly depends on the doping element, the coating deposition process and the test conditions. The formation of metal carbide phases during annealing is an important factor that increases the thermal stability of the metal-doped DLC coating when compared to the pure DLC coating. The metal carbide phases stabilise the diamond-like structure at elevated temperature and thus the graphitisation is delayed. As found from the literature, the graphitisation can be delayed up to ~500°C if Mo, W or Si is used as doping element.

Mo and W are two important doping elements that improve the thermal stability of the DLC coating and simultaneously provide benefit to the tribological properties. A carbon-based coating doped with both Mo and W has been developed in order to provide low friction and improved wear resistance at ambient as well as in elevated temperature. The development of Mo − W doped carbon-based coating (Mo−W−C) and its improved tribological properties at ambient condition were explained in detail elsewhere [11]. This paper investigates the oxidation behaviour of Mo−W−C coating at elevated temperature using dynamic and isothermal oxidation tests and compares the performance with a state-of-the-art DLC coating.

2. Experimental Details

2.1. Coating deposition process

The Mo − W doped carbon-based coating (Mo−W−C) was deposited on 304 stainless steel coupons (15 mm × 50 mm × 0.8 mm) by combined High Power Impulse Magnetron Sputtering (HIPIMS) and Unbalanced Magnetron Sputtering (UBM) techniques in an

industrial sized HTC 1000−4 PVD coating machine enabled with HIPIMS technology. More details on deposition process and the properties of as-deposited coating were explained elsewhere. The dense coating microstructure and excellent adhesion strength (L_c~80.8 N) were attributed to the use of HIPIMS technique during coating deposition. The ~2.2 µm thick coating architecture consisted of a HIPIMS − treated interface, a thin Mo − W − N base layer and a Mo − W − C layer on the top [11]. The oxidation resistance of Mo−W−C coating during isothermal and dynamic tests is compared with a commercially available state-of-the-art DLC coating. The ~3 µm thick DLC coating was deposited on the same steel coupons by combined PVD and PACVD processes. The coating architecture contained a Cr base layer, followed by a sputtered Cr-WC adhesion layer, a W:C−H intermediate layer and an a:C−H layer on the top. Thus the DLC coating is expressed as $\mathrm{DLC}\left(\mathrm{Cr}\,/\,\mathrm{Cr}-\mathrm{WC}\,/\,\mathrm{W}:\mathrm{C}-\mathrm{H}\,/\,\mathrm{a}:\mathrm{C}-\mathrm{H}\right)$ in this article.

2.2. Oxidation tests: isothermal and dynamic

The isothermal oxidation tests were performed in the furnace. The Mo−W−C coated samples were heated from room temperature (~25°C) to the pre-set temperatures ranging from 400°C − 800°C with a step of 100°C at ambient atmosphere. Once the pre-set temperature was reached, the samples were heated at that temperature for 2 hours in order to achieve proper oxidation and then cooled slowly in air. Same heat-treatment was carried out for the $\mathrm{DLC}\left(\mathrm{Cr}\,/\,\mathrm{Cr}-\mathrm{WC}\,/\,\mathrm{W}:\mathrm{C}-\mathrm{H}\,/\,\mathrm{a}:\mathrm{C}-\mathrm{H}\right)$ coated samples up to 500°C and no tests were continued at higher temperatures due to local delamination of the coating at 500°C.

The dynamic oxidation tests were carried out using a high performance modular Thermo-Gravimetric Analyser (TGA) from SETARAM instrumentation. The Mo−W−C and

$DLC(Cr/Cr-WC/W:C-H/a:C-H)$ coated coupons were suspended from the microbalance and heated from room temperature (20°C) to a pre-set value (1000°C) at a heating rate of 1°C per minute. Slow heating rate was preferred to monitor any distinguishable changes of sample weight during oxidation. The total duration of the test was 11 hours including the cooling phase after reaching the maximum test temperature of 1000°C. The resultant curve showing the mass change against the furnace temperature was plotted with the help of SETSYS software associated with the instrument.

2.3.   Characterisation techniques

The oxidation behaviour of Mo−W−C and $DLC(Cr/Cr-WC/W:C-H/a:C-H)$ coatings was investigated using scanning electron microscopy (SEM), surface profilometer, X-ray diffraction (XRD) and Raman spectroscopy. The topographical imaging was carried out by secondary electron detector (ETD) of a fully computerised FEI NOVA NANOSEM 200 coupled with Energy Dispersive X-ray (EDX) analysis module (Oxford instruments X-max detector with INCA analysis software). A surface profilometer (DEKTAK 150) was used to measure the surface roughness of the oxidised samples. For each scan, the probe travelled 1000 µm length of the surface profile in 120 s and the surface roughness of the scanned profile was calculated by the associated software. The scanning was repeated for 8 − 10 times for each oxidised sample and their average was considered. The X-ray mapping was done on the fractured cross-section of the heat-treated Mo−W−C and $DLC(Cr/Cr-WC/W:C-H/a:C-H)$ coated samples in order to identify the distribution of elements along the coating thickness. The phase composition of the oxidised samples was studied using X-ray diffraction (XRD) and Raman spectroscopy. The XRD analysis was carried out with a PANalytical Empyrean PIXcel 3D automated diffractometer

using Bragg-Brentano and glancing angle geometry. The scanning range was selected as $2\theta = 20° − 130°$ for Bragg-Brentano geometry and $2\theta = 20° − 120°$ for glancing angle geometry with an incident angle of 2°. The X-ray source was Cu−Kα radiation with a wavelength of 1.54 nm. The Raman spectrum was collected from random positions on the oxidised surfaces using a Horiba-Jobin-Yvon LabRam HR800 integrated Raman spectrometer fitted with green laser of wavelength 532 nm. A 10% transmission filter was used to reduce the intensity of incident beam to avoid the damage due to irradiation. The samples were exposed to the laser for 120 seconds for spectrum collection and the collected spectra were averaged over 5 acquisitions in the wavelength range of $50 − 2250 \ cm^{-1}$. During analysis, the background of spectrum was corrected using a 2nd order polynomial whereas a multi-peak Gaussian-fitting function was used to deconvolute the spectrum and identify the Raman peaks. More details on the parameters used during experiment and the spectrum analysis were described elsewhere [12].

3. Results and Discussion

3.1. Isothermal oxidation behaviour of Mo−W−C coating

3.1.1. Surface morphology and coating microstructure

Figures 1−6 show the surface morphology and microstructure of as-deposited Mo−W−C coating and after heat-treated to 400°C − 800°C. Figure 1a shows smooth surface of the as-deposited coating and figure 1b shows the X-ray mapping done on the fracture cross-section of the coating in order to understand the elemental distribution across the coating thickness. The yellow outline on the SEM image indicates the cross-sectional area on which X-ray mapping is done. The as-deposited coating architecture consists of a thin Mo − W − N base layer (average thickness ~130 nm) adjacent to the Si substrate, followed by a thick (~2.2 μm)

and dense columnar Mo − W − C layer on the top. Carbon concentration is observed to be high at the top coating layer compared to Mo and W. The doping elements are uniformly distributed throughout the entire coating thickness, but their presence, as expected, is higher in the Mo − W − N base layer [11].

A significant change in surface morphology is observed (figure 2a) due to the development of metal carbide phases at 400°C (later confirmed by XRD and Raman analyses). Figure 2b shows the X-ray mapping carried out on the cross-section of the sample heat-treated to 400°C. The columnar microstructure of as-deposited coating becomes smooth after heat-treatment and no change in coating thickness (~2.2 μm) is observed. The as-deposited coating retains its elemental composition (Mo, W and C) at 400°C and no trace of oxygen is found in the coating. No outward diffusion of substrate elements (such as Cr and Fe) into the coating is observed indicating no effect of temperature on the as-deposited coating at 400°C.

The SEM image in figure 3a shows the surface morphology of the sample oxidised at 500°C. A thin and dense metal oxide layer is formed at this temperature, which uniformly covers the coating surface. Figure 3b shows the X-ray mapping done on the cross-section of the heat-treated sample. The strong presence of Mo, W and C is observed along with a little amount of oxygen uniformly distributed within the coating material. An outward diffusion of Cr and Fe is also present at 500°C indicating this temperature can be considered as an onset of the coating oxidation. The coating thickness (~2 μm) is found almost unchanged, which indicates that the oxidation processes are still in their initial stages.

The SEM image in figure 4a shows the formation of a thick oxide layer that covers the entire surface exposed to the environment at 600°C. The cross-section image in figure 4b reveals

that the total oxide scale thickness is ~3.6 µm due to the volume expansion of the oxide material. The Mo−W−C coating can be still observed as a thin (~500 nm) layer underneath of the metal oxide layer which indicates that the coating material has been almost fully consumed and converted to a mixed oxide scale. The X-ray mapping in figure 4b further supports these observations by showing significant presence of oxygen in the scale along with Mo and W. However, few metal carbide phases (tungsten and molybdenum carbides) are still retained inside the oxide scale as indicated by the carbon map. The outward diffusion of substrate elements like Cr and Fe into the oxide scale is clearly visible.

The metal oxide growth becomes significant at 700°C resulting in an irregular surface features as seen in figure 5a. The X-ray mapping results in figure 5b show strong presence of W and oxygen in the scale indicating formation of tungsten oxides. As reported in the literature, molybdenum oxide (MoO_3) starts to evaporate after 600°C [13], thus the concentration of Mo is found significantly low at 700°C. Diffusion of substrate elements such as Cr and Fe into the coating is observed, which leads to formation of iron and chromium oxides and possibly chromium carbide. This fact is supported by the formation of a very thin carbon rich layer on the top of metal oxide scale as observed in the X-ray maps. The presence of this metal carbide layer is still found after isothermal heat-treatment of 2 hours, however it is expected that this layer will be oxidised if the heat-treatment is continued for several more hours. The metal oxides are formed in two separate layers as indicated in the SEM image of figure 5b and as a result, the total oxide scale thickness is increased to ~4.2 µm.

Figure 6a shows that the oxidation processes are further enhanced at 800°C. A thick metal oxide layer is formed which covers the surface by large islands of oxides due to the oxide scale growth mechanism. This is further supported by the strong presence of oxygen in the X-

ray map as shown in figure 6b. At this temperature, Mo is almost depleted from the coating due to rapid evaporation of molybdenum oxides [13]. Furthermore as the onset of sublimation of tungsten oxide is at 750°C [14], the top surface of the oxide scale becomes depleted of tungsten. Apart from compositional changes, the sublimation of both Mo and W based oxides at this high temperature (800°C) leads to a reduction of thickness of the oxide scale to ~3.3 μm. Despite the sublimation process however, the X-ray map clearly shows that the remaining oxide scale at predominantly consists of tungsten oxides. Similar to the 700°C case, Carbon has been mapped in a thin top layer where it exists in a form of carbide phases. Both W and Mo are known as a strong carbide forming elements which together with the Cr which is out-diffused from the substrate. While the tungsten and molybdenum oxides are volatile at 800°C, the top surface becomes richer to metal carbides. At this temperature the carbides itself will oxidise via gradual replacement of carbon atoms by oxygen atoms where the extent of oxidation depends on the exposure time. In parallel, the outward diffusion of substrate elements continues to produce a mixture of iron and chromium oxides along with the tungsten and molybdenum oxides.

The metal oxide growth during isothermal heat-treatment deteriorates the surface finish of as-deposited Mo−W−C coating as shown in figure 7. The average surface roughness (R_a) of as-deposited coating is ~0.07 μm, which increases to ~0.12 μm due to formation of crystalline structure at 400°C. With further rise in temperature up to 600°C, a slight decrease in average surface roughness ($R_a = 0.06 − 0.08$ μm) is observed due to insignificant metal oxide growth. The oxide growth becomes significant as the temperature reaches to 700°C. As a result, an irregular surface is formed and a sudden rise in average surface roughness ($R_a = 0.29$ μm) is observed. At 800°C, the oxidation becomes rapid leading to further increase in average surface roughness ($R_a = 0.36$ μm) due to the volume expansion of the oxide phase.

3.1.2.   Phase composition using X-ray diffraction

Figure 8a shows the XRD patterns collected using Bragg-Brentano geometry indicating the change in phase composition of as-deposited Mo−W−C coating and after isothermal heat-treatment at 400°C and 500°C in air. The XRD pattern of the as-deposited coating shows that the coating structure is a mixture of amorphous carbon and metal carbides namely WC, W_2C, and Mo_2C. When heat-treated to 400°C, the carbidisation process develops further to produce more metal carbide phases (W_2C and Mo_2C). No metal oxide phases are appeared in the XRD pattern indicating absolutely no oxidation occurs at 400°C. The metal carbide phases are retained up to 500°C; however small amount of metal oxides such as WO_3, W_5O_{14} and MoO_3 is also observed in the XRD pattern indicating that the 500°C temperature can be defined as onset of oxidation for Mo−W−C coating. Although outward diffusion of substrate elements such as Fe and Cr have been observed by X-ray mapping (figure 3b) at 500°C, but no crystallographic phases based on these elements are detected by the XRD analyses possibly due to their small amount.

A complete change in the shape of the XRD patterns is observed when Mo−W−C coating is heat-treated in the temperature range of 600°C − 800°C (figure 8b). At 600°C, most of the metal carbide phases are transformed to different tungsten oxides (such as principal oxide WO_3 and intermediate oxides W_5O_{14} and $W_{18}O_{49}$) and molybdenum oxides (such as principal oxide MoO_3 and intermediate oxides Mo_9O_{26} and $Mo_{17}O_{47}$) indicated in the XRD pattern as W_xO_y and Mo_xO_y respectively. Few tungsten carbide phases (WC and W_2C) are also observed in the XRD pattern forming a mixture with the oxide scale. Similarly to the 500°C case, no oxides of substrate elements (Fe and Cr) are detected by the XRD analyses at 600°C.

The XRD pattern of the coating exposed to 700°C shows a significant decrease in Mo_xO_y peak intensities (figure 8b) due to the sublimation of the Mo_xO_y. No significant change in the intensities of the W_xO_y peaks is observed indicating their stability at this temperature. The exposure of coating to 700°C leads to significant out-diffusion and oxidation of substrate elements to form Fe_2O_3 and Cr_2O_3 phases. The tungsten carbide phases (WC and W_2C) are still retained inside the oxide scale however, the intensity is reduced.

Upon exposure to 800°C, no W_xO_y and Mo_xO_y peaks in the 2θ range of ~23°, ~38° and 44° − 49° are detected due to the increase sublimation rate of the metal oxides. A rapid decrease in rest of the W_xO_y and Mo_xO_y peak intensities is observed and new peaks appear due to the formation of WO_2 and MoO_2 via reduction of W_xO_y and Mo_xO_y phases. The WC peak at ~31.5° is still retained but the intensity is significantly reduced. The W_2C peak at ~52.3° is totally disappeared due to severe oxidation of the coating. The Fe_2O_3, Cr_2O_3 and chromium carbide ($Cr_{23}C_6$, Cr_3C_2) peaks are detected in the XRD pattern indicating exposure of the substrate. These results clearly support the findings of X-ray mapping as earlier discussed in section 3.1.1.

For better understanding of the oxidation behaviour up to 600°C, the changes in phase composition of Mo−W−C coating are investigated by XRD analyses using glancing angle geometry (GAXRD). Figure 9a shows the GAXRD patterns of the coating in as-deposited condition and after oxidised to 400°C. A single broad peak is observed in the GAXRD pattern of the as-deposited coating indicating its nanocrystalline almost X-ray amorphous structure and the presence of hexagonal WC [1 0 0], W_2C [0 0 2] and Mo_2C [0 0 2] phases [11]. When heated to 400°C, the W_2C [0 0 2] and Mo_2C [0 0 2] phases are retained and the peak intensity is significantly increased due to the formation of more metal carbide phases.

Two new peaks are appeared indicating the presence of hexagonal W_2C [1 0 2] and W_2C [1 1 2] phases. As a result, the nanocrystalline structure of the as-deposited coating is transformed into crystalline structure at 400°C. This causes a significant change in surface morphology of the heat-treated coating as observed in figure 2a. No metal oxide phases are found in the GAXRD pattern, which confirms that absolutely no oxidation occurs for Mo−W−C coating at 400°C and supports the findings of X-ray mapping and XRD analyses using Bragg-Brentano geometry.

Figure 9b shows the GAXRD patterns of the Mo−W−C coating oxidised to 500°C and 600°C respectively. The hexagonal W_2C [0 0 2] phase is retained up to 500°C; however the peak intensity is rapidly decreased. The rest of the metal carbides react with oxygen at 500°C and form an oxide layer containing MoO_3 and different tungsten oxides $[W_xO_y \rightarrow WO_3 + W_5O_{14} + W_{18}O_{49}]$. A complete change in GAXRD pattern shape is observed at 600°C due to conversion of the coating to a mixed metal oxide scale containing different tungsten oxides $[W_xO_y \rightarrow WO_3 + W_5O_{14} + W_{18}O_{49}]$ and molybdenum oxides $[Mo_xO_y \rightarrow MoO_3 + Mo_9O_{26} + Mo_{17}O_{47}]$. As a result, the peak intensities of W_xO_y and Mo_xO_y are significantly increased. The WC [0 0 1] phase is still retained inside the oxide scale as observed in the XRD pattern at ~31.5°. Moreover the absence of iron and chromium oxides confirms that the substrate remains unexposed at 600°C. These findings support the results obtained from X-ray mapping and XRD patterns collected using Bragg-Brentano geometry.

3.1.3. Phase composition using Raman spectroscopy

Figure 10a shows the Raman spectra collected from the as-deposited Mo−W−C coating and after heat-treated to 400°C and 500°C. The as-deposited coating contains distinct disordered

(D) and sp^2 bonded graphitic carbon (G) peaks and Mo$_2$C peaks. The I$_D$/I$_G$ ratio is found as 1.96. More details on the Raman analysis of the as-deposited coating has been described elsewhere [11]. When heated to 400°C, the Mo$_2$C peak and the graphitic carbon peaks are retained and a strong WC peak is observed. This completely agrees with the findings of the XRD patterns that the metal carbide phases are developed at 400°C (figures 8a and 9a). The development of metal carbide phases decreases the amount of free graphitic carbon present in the coating. Thus the I$_D$/I$_G$ ratio slightly decreases to 1.64 at 400°C indicating the decrease in disordering of carbon−carbon bonds in the coating.
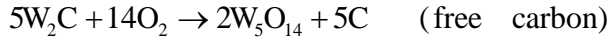
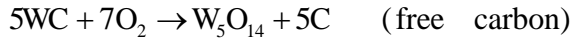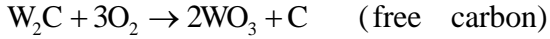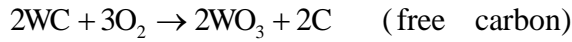As the temperature rises to 500°C, the graphitic peaks are retained along with few metal carbide phases and rest of the metal carbide phases are oxidised indicating initial oxidation of Mo−W−C coating (figure 10a). After deconvolution of the spectrum, the WC and Mo$_2$C peaks are found along with W$_x$O$_y$ [W$_x$O$_y$ → WO$_3$ + W$_{18}$O$_{49}$ + W$_{20}$O$_{58}$] and Mo$_x$O$_y$ [Mo$_x$O$_y$ → MoO$_3$ + Mo$_4$O$_{11}$ + Mo$_5$O$_{14}$ + Mo$_8$O$_{23}$] peaks. The formation of this metal oxide layer on the surface prevents depletion of free carbon from the coating. As a result, the I$_D$/I$_G$ ratio rises to 2.4 establishing coating's graphitic nature at 500°C. This increase in I$_D$/I$_G$ ratio from 400°C to 500°C indicates an increase in disordering of carbon−carbon bonds in the coating due to heat-treatment. This is further supported by the upshifting of G peak position of the as-deposited coating (1574.32 cm^{-1}) after heat-treatment (1589.38 cm^{-1} and 1586.63 cm^{-1} when heated to 400°C and 500°C respectively). Table 1 lists the Raman peaks of the metal carbides and metal oxides present in Mo−W−C coating after heat-treated to 400°C and 500°C. Those peaks available in the literature [15 − 22] are also documented in the same table.

Figure 10b shows the Raman spectra collected from the Mo−W−C coating after heat-treatment in the temperature range of 600°C − 800°C. The D and G peaks are disappeared at
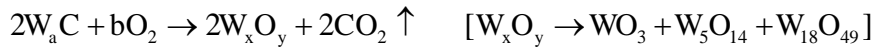
600°C indicating loss of coating's graphitic nature. A complete change in the shape of the spectrum is observed due to severe oxidation of the coating. The WC peak is retained along with W_xO_y $[W_xO_y \rightarrow WO_3 + W_{18}O_{49} + W_{20}O_{58}]$ and Mo_xO_y $[Mo_xO_y \rightarrow MoO_3 + Mo_4O_{11} + Mo_5O_{14} + Mo_8O_{23}]$ peaks. The absence of metal oxide peaks from the substrate confirms no substrate exposure at 600°C. At 700°C, the evaporation of Mo_xO_y decreases the respective peak intensities and eventually exposes the substrate as indicated by the presence of Fe_2O_3 and CrO_2 peaks. At 800°C, both W_xO_y and Mo_xO_y are vaporised leading to a significant decrease in the respective peak intensities; however the spectrum is magnified 10 times during plotting for better visualisation. The substrate is severely oxidised at 800°C as indicated by the presence of Fe_2O_3, Cr_2O_3, CrO_2 and Cr_2C peaks in the spectrum. The WC peak is observed in the spectrum up to 800°C, however its intensity is significantly decreased with rise in temperature. Tables 2 − 4 list the Raman peaks of the metal carbides and metal oxides present in the Mo−W−C coating after heat-treated to 600°C − 800°C. Those peaks available in the literature [15 − 26] are also documented in the respective tables. As understood from the results obtained from XRD and Raman analyses, the possible chemical reactions occurred during isothermal oxidation of Mo−W−C coating are listed in the equation set (1):
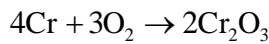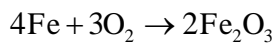
- 400°C: Development of metal carbide phases and NO oxidation of $Mo-W-C$ coating
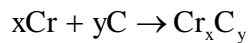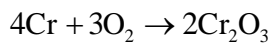
- 500°C: Onset of oxidation

$2WC + 3O_2 \rightarrow 2WO_3 + 2C$ (free carbon)

$W_2C + 3O_2 \rightarrow 2WO_3 + C$ (free carbon)

$5WC + 7O_2 \rightarrow W_5O_{14} + 5C$ (free carbon)

$5W_2C + 14O_2 \rightarrow 2W_5O_{14} + 5C$ (free carbon)

$Mo_2C + 3O_2 \rightarrow 2MoO_3 + C$ (free carbon)

- 600°C: Oxidation continues

$2W_aC + bO_2 \rightarrow 2W_xO_y + 2CO_2 \uparrow$ $[W_xO_y \rightarrow WO_3 + W_5O_{14} + W_{18}O_{49}]$

$2Mo_aC + bO_2 \rightarrow 2Mo_xO_y + 2CO_2 \uparrow$ $[Mo_xO_y \rightarrow MoO_3 + Mo_9O_{26} + Mo_{17}O_{47}]$
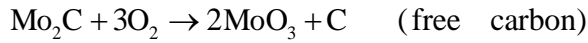
- 700°C : Oxidation continues and exposure of substrate

$W_xO_y \rightarrow stable$ but $Mo_xO_y \rightarrow evaporates$

$2W_aC + bO_2 \rightarrow 2W_xO_y + 2CO_2 \uparrow$ $[W_xO_y \rightarrow WO_3 + W_5O_{14} + W_{18}O_{49}]$

$2Mo_aC + bO_2 \rightarrow 2Mo_xO_y + 2CO_2 \uparrow$ $[Mo_xO_y \rightarrow MoO_3 + Mo_9O_{26} + Mo_{17}O_{47}]$

$4Fe + 3O_2 \rightarrow 2Fe_2O_3$

$4Cr + 3O_2 \rightarrow 2Cr_2O_3$

- 800°C : Severe oxidation of both the coating and the substrate

$W_xO_y \rightarrow evaporates$ and   remaining $Mo_xO_y \rightarrow melts$

$2W_aC + bO_2 \rightarrow 2W_xO_y + 2CO_2 \uparrow$ $[W_xO_y \rightarrow WO_3 + W_5O_{14} + W_{18}O_{49} + WO_2]$

$2Mo_aC + bO_2 \rightarrow 2Mo_xO_y + 2CO_2 \uparrow$ $[Mo_xO_y \rightarrow MoO_3 + Mo_9O_{26} + Mo_{17}O_{47} + MoO_2]$

$4Fe + 3O_2 \rightarrow 2Fe_2O_3$

$4Cr + 3O_2 \rightarrow 2Cr_2O_3$
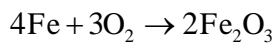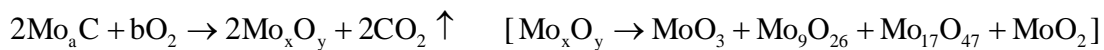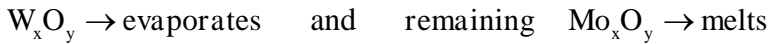
$xCr + yC \rightarrow Cr_xC_y$ (1)

3.2. Isothermal oxidation behaviour of DLC (Cr/Cr-WC/W:C−H /a:C−H) coating

3.2.1. Surface morphology and coating microstructure

Figure 11a shows no significant change in the surface morphology of as-deposited $\mathrm{DLC}\left(\mathrm{Cr}/\mathrm{Cr}-\mathrm{WC}/\mathrm{W}:\mathrm{C}-\mathrm{H}/\mathrm{a}:\mathrm{C}-\mathrm{H}\right)$ coating after oxidised to 400°C. The smooth surface of the as-deposited coating (R_a = 0.08 μm) remains similar at 400°C (R_a = 0.05 μm). Figure 11b shows the X-ray mapping done on the cross-section of the heat-treated sample. The maps reveal strong presence of carbon at the top of the coating and a mixture of carbon and tungsten in the intermediate layer. The diffusion of substrate elements (Fe and Cr) into the coating is also observed at 400°C. Oxygen is present throughout the coating thickness as well as into the substrate indicating that the coating does not provide secure protection against oxidation at 400°C. The coating thickness (~3 μm) is found to be almost same as the as-deposited coating.

Figure 12a shows the surface morphology of $\mathrm{DLC}\left(\mathrm{Cr}/\mathrm{Cr}-\mathrm{WC}/\mathrm{W}:\mathrm{C}-\mathrm{H}/\mathrm{a}:\mathrm{C}-\mathrm{H}\right)$ coating at 500°C. At this temperature the substrate surface is locally exposed whereas the remaining area is covered by porous oxide layer as understood from the X-ray maps. The maps in figure 12b show complete absence of carbon but presence of W and oxygen, which confirms that the substrate is only partially covered by W-based oxide layer. The substrate itself is fully oxidised on the surface as confirmed by the Fe and oxygen maps. The local surface exposure can be due to two processes developing in parallel. On one hand, the exposure temperature is high enough to trigger the formation of gaseous hydrogen, CH_x and CO_2 compounds. In parallel, the oxidation of W:C−H layer and outward diffusion of Fe produces different oxides, which lead to delamination of the top carbon layer and subsequent substrate exposure due to their volume expansion.
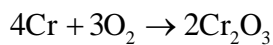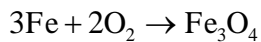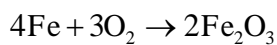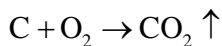
3.2.2. Phase composition using X-ray diffraction and Raman spectroscopy

The change in phase composition of $\mathrm{DLC}\left(\mathrm{Cr/Cr-WC/W:C-H/a:C-H}\right)$ coating during isothermal oxidation (up to 500°C) is investigated by XRD analyses using Bragg-Brentano geometry as shown in figure 13. The as-deposited coating contains two dominant peaks at ~44.5° and ~66.4° (labelled as 'a' and 'b' respectively in the XRD pattern) due to the hydrogenated amorphous top layer (a:C−H), whereas WC [1 0 0] and W_2C [1 0 1] peaks are observed due to the W:C−H intermediate layer. When exposed to 400°C, the a:C−H top layer releases hydrogen and gaseous CH_x species and thus exposes the intermediate W:C−H layer. As a result, the 'a' and 'b' peaks are completely disappeared and different tungsten oxide peaks $[W_xO_y \rightarrow WO_3 + WO_2 + W_5O_{14} + W_{18}O_{49}]$ are formed. The Fe_2O_3 and Cr_2O_3 peaks are observed in the XRD pattern indicating oxidation of substrate and the base layer. The a:C−H top layer is completely depleted at 500°C and further oxidation of W:C−H layer exposes the substrate. As a result, dominant W_xO_y, Fe_2O_3 and Cr_2O_3 peaks are appeared in the XRD pattern. These observations further support the findings with the X-ray mapping as discussed in the previous section.
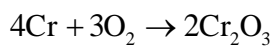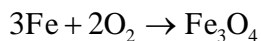
Figure 14 shows the Raman spectra collected from the as-deposited $\mathrm{DLC}\left(\mathrm{Cr/Cr-WC/W:C-H/a:C-H}\right)$ coating and after isothermal oxidation at 400°C and 500°C. The as-deposited coating contains significant amount of sp^3 bonded carbon, thus the spectrum is dominated by the G peak indicating its amorphous, diamond-like structure. The I_D/I_G ratio is found as 0.59 (figure 'a' in the inset). When heated to 400°C, the sp^3 bonded carbons are converted into sp^2 bonded carbons (i.e. the graphitisation starts) leading to significant increase in D peak intensity. As a result, I_D/I_G ratio rapidly increases to 1.01

(figure 'b' in the inset). Upon further heating up to 500°C, a distinct disordered peak is appeared in the spectrum indicating complete transformation of diamond-like structure into the graphite-like structure. Thus the I_D/I_G ratio further increases to 1.04 (figure 'c' in the inset). This gradual increase in I_D/I_G ratio indicates the rise in ordering of DLC coating with increase in temperature. This is further supported by the upshifting of the G peak position of the as-deposited coating (1545.89 cm^{-1}) after heat-treatment (1574.32 cm^{-1} and 1583.28 cm^{-1} when heated to 400°C and 500°C respectively). The initiation of graphitisation at 400°C confirms poor thermal stability of the $DLC\left(Cr\,/\,Cr-WC\,/\,W:C-H\,/\,a:C-H\right)$ coating compared to the Mo−W−C coating. As understood from the results obtained from XRD and Raman analyses, the possible chemical reactions occurred during isothermal oxidation of $DLC\left(Cr\,/\,Cr-WC\,/\,W:C-H\,/\,a:C-H\right)$ coating are listed in the equation set (2):

- 400°C: oxidation initiates and substrate marginally exposed

$$a:C-H\,(\text{top-layer}) \xrightarrow{\text{heating}} CH_x \uparrow + H_2 \uparrow$$
$$W:C-H\,(\text{intermediate-layer}) + O_2 \rightarrow W_xO_y + CH_x \uparrow + CO_2 \uparrow$$
$$\text{where} \quad W_xO_y \rightarrow W_5O_{14} + W_{18}O_{49} + WO_2$$
$$C + O_2 \rightarrow CO_2 \uparrow$$
$$4Fe + 3O_2 \rightarrow 2Fe_2O_3$$
$$3Fe + 2O_2 \rightarrow Fe_3O_4$$
$$4Cr + 3O_2 \rightarrow 2Cr_2O_3$$
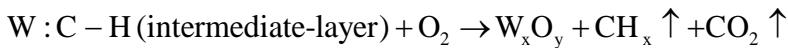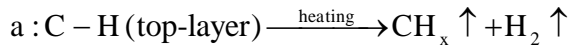
- 500°C: severe oxidation and substrate completely exposed
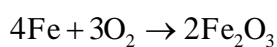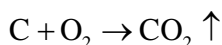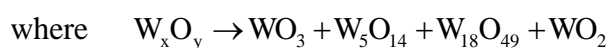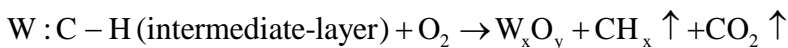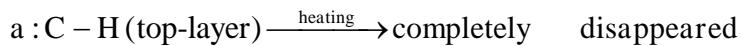
$$a:C-H\,(\text{top-layer}) \xrightarrow{\text{heating}} \text{completely} \quad \text{disappeared}$$
$$W:C-H\,(\text{intermediate-layer}) + O_2 \rightarrow W_xO_y + CH_x \uparrow + CO_2 \uparrow$$
$$\text{where} \quad W_xO_y \rightarrow WO_3 + W_5O_{14} + W_{18}O_{49} + WO_2$$
$$C + O_2 \rightarrow CO_2 \uparrow$$
$$4Fe + 3O_2 \rightarrow 2Fe_2O_3$$
$$3Fe + 2O_2 \rightarrow Fe_3O_4$$
$$4Cr + 3O_2 \rightarrow 2Cr_2O_3 \tag{2}$$

3.3. Thermo-gravimetric analysis (TGA) of Mo−W−C and DLC (Cr/Cr-WC/W:C−H /a:C−H) coatings

Figure 15 shows the dynamic oxidation behaviour of Mo−W−C and $\text{DLC}\left(\text{Cr}/\text{Cr}-\text{WC}/\text{W}:\text{C}-\text{H}/\text{a}:\text{C}-\text{H}\right)$ coatings as obtained from thermo-gravimetric analysis. The Mo−W−C coating shows no change in mass up to ~600°C, followed by a slight increase in mass gain to ~3 mg when heated up to ~800°C. Further rise in the temperature up to ~1000°C results in rapid and large mass gain (~23 mg) due to the formation of heavy metal oxides. The image of the coated sample and the magnified image of the oxidised surface (provided in the inset) indicate no delamination of the coating during the test because of its strong metallurgical bond with the substrate. It is already published that plasma generated in HIPIMS contains a high amount of metal ions, which are implanted into the interface region and promote strong metallurgical bonds between coating and the substrate. These bonds are so strong that they align the orientation of coating growth towards the orientation of crystals in the substrate in at least one direction. Thus over few micro meters area, the coating duplicates the substrate structure. As a result, the adhesion significantly increases and prevents delamination of the coating [27].

On the other hand, mass of the $\text{DLC}\left(\text{Cr}/\text{Cr}-\text{WC}/\text{W}:\text{C}-\text{H}/\text{a}:\text{C}-\text{H}\right)$ coated sample remains constant up to ~380°C however further heating up to ~650°C results in gradual decrease of the mass at a rate of ~5 mg°C^{-1}. This mass loss is due to the evaporation and local delamination of the $\text{DLC}\left(\text{Cr}/\text{Cr}-\text{WC}/\text{W}:\text{C}-\text{H}/\text{a}:\text{C}-\text{H}\right)$ coating as described in section 3.2. The image of the $\text{DLC}\left(\text{Cr}/\text{Cr}-\text{WC}/\text{W}:\text{C}-\text{H}/\text{a}:\text{C}-\text{H}\right)$ coated sample and the magnified image of the oxidised surface (provided in the inset) shows delamination of the coating due to the volume expansion of the oxide layer. As a result, the surface roughness of

the $DLC(Cr/Cr-WC/W:C-H/a:C-H)$ coated sample is found much higher ($R_a = 0.4$ μm) compared to the Mo−W−C coated sample (R_a = 0.27 μm). Overall, the thermo-gravimetric analysis indicates that the Mo−W−C and $DLC(Cr/Cr-WC/W:C-H/a:C-H)$ coatings resist oxidation up to ~800°C and ~380°C respectively and further heat-treatment significantly degrades the coating properties.

It should be noted that the delamination occurs for $DLC(Cr/Cr-WC/W:C-H/a:C-H)$ coating at ~380°C during thermo-gravimetric test, however no delamination occurs for the same coating when isothermally heated to 400°C. The coating was heat-treated for 2 hours during isothermal test whereas a slow heating rate like 1°C per minute takes more than 6 hours to reach 380°C during thermo-gravimetric test. Therefore, long exposure time of 6 hours leads to local delamination of the coating at ~380°C.

4. Conclusions

The oxidation behaviour of Mo−W doped carbon-based coating (Mo−W−C) is investigated in isothermal and dynamic conditions and the performance is compared against a state-of-the-art $DLC(Cr/Cr-WC/W:C-H/a:C-H)$ coating. The isothermal tests are carried out in the temperature range of 400°C − 800°C in furnace, whereas the temperature is increased from ambient to 1000°C at a heating rate of 1°C per minute for the dynamic tests (TGA). The conclusions drawn from this study are as follows:

- The nanocrystalline structure of the as-deposited Mo−W−C coating is transformed into crystalline structure due to the development of metal carbide phases at 400°C. Analytical techniques confirm that no oxidation occurs at 400°C. The oxidation process initiates at 500°C, however coating's graphitic nature is still preserved. Further progress of oxidation process up to 700°C forms a thicker mixed oxide scale and at 800°C, severe oxidation of both the coating and the substrate are clearly observed.

- The graphitisation of $DLC\left(Cr / Cr - WC / W : C - H / a : C - H\right)$ coating is observed at 400°C. The diamond-like structure is completely converted into the soft graphite-like structure at 500°C. Simultaneously, the top hydrogenated carbon layer is totally disappeared due to formation of gaseous CH_x and CO_2 compounds, followed by the local delamination of the coating due to volume expansion of oxides from W:C−H layer and substrate.

- During isothermal tests, the initial oxidation of Mo−W−C coating is observed at 500°C however it's as-deposited graphitic nature is retained. On the other hand, the state-of-the-art $DLC\left(Cr / Cr - WC / W : C - H / a : C - H\right)$ coating is locally delaminated at this temperature and simultaneously the diamond-like structure is completely converted into the soft graphite-like structure. This indicates its improved oxidation resistance of Mo−W−C coating compared to $DLC\left(Cr / Cr - WC / W : C - H / a : C - H\right)$ coating.

- The thermo-gravimetric test results show that the Mo−W−C coating resists oxidation up to ~800°C and no coating delamination is observed because of its strong metallurgical bond with the substrate. Alternatively, local delamination of the state-of-the-art

$\mathrm{DLC}\left(\mathrm{Cr}/\mathrm{Cr}-\mathrm{WC}/\mathrm{W}:\mathrm{C}-\mathrm{H}/\mathrm{a}:\mathrm{C}-\mathrm{H}\right)$ coating is observed beyond ~380°C. This confirms improved thermal stability of the Mo−W−C coating compared to the $\mathrm{DLC}\left(\mathrm{Cr}/\mathrm{Cr}-\mathrm{WC}/\mathrm{W}:\mathrm{C}-\mathrm{H}/\mathrm{a}:\mathrm{C}-\mathrm{H}\right)$ coating in dynamic condition.

References

[1] D.R. Tallant, J.E. Parmeter, M.P. Siegal, R.L. Simpson, The thermal stability of diamond-like carbon, Diamond and Related Materials, 4 (1995) 191-199

[2] G. Ma, S. Gong, G. Lin, L. Zhang, G. Sun, A study of structure and properties of Ti-doped DLC film by reactive magnetron sputtering with ion implantation, Applied Surface Science, 258 (2012) 3045–3050

[3] D. Y. Wang, C. L. Chang, W. Y. Ho, Oxidation behaviour of diamond-like carbon films, Surface and Coatings Technology, 120–121 (1999) 138–144

[4] S. Zhang, X. L. Bui, X. Li, Thermal stability and oxidation properties of magnetron sputtered diamond-like carbon and its nanocomposite coatings, Diamond & Related Materials, 15 (2006) 972–976

[5] B. Yang, Y. Zheng, B. Zhang, L. Wei, J. Zhang, The high-temperature tribological properties of Si-DLC films, Surface and Interface Analysis, 44 (2012) 1601–1605

[6] W. J. Wu, M. H. Hon, Thermal stability of diamond-like carbon films with added silicon, Surface and Coatings Technology, 111 (1999) 134–140

[7] S.S. Camargo Jr, A.L. Baia Neto, R.A. Santos, F.L. Freire Jr, R. Carius, F. Finger, Improved high-temperature stability of Si incorporated a-C:H films, Diamond and Related Materials, 7 (1998) 1155–1162

[8] M.C. Chiu, W.P. Hsieh, W.Y. Ho, D. Y. Wang, F.S. Shieu, Thermal stability of Cr-doped diamond-like carbon films synthesized by cathodic arc evaporation, Thin Solid Films, 476 (2005) 258– 263

[9] Y.N. Kok, P.Eh. Hovsepian, Resistance of nanoscale multilayer C/Cr coatings against environmental attack, Surface & Coatings Technology, 201 (2006) 3596–3605

[10] R.K.Y. Fu, Y.F. Mei, M.Y. Fu, X.Y. Liu, P.K. Chu, Thermal stability of metal-doped diamond-like carbon fabricated by dual plasma deposition, Diamond & Related Materials, 14 (2005) 1489 – 1493

[11] P. Mandal, A.P. Ehiasarian, P. Eh. Hovsepian, Tribological behaviour of Mo − W doped carbon-based coating at ambient condition, Tribology International, 90 (2015) 135–147

[12] P. Mandal, A.P. Ehiasarian, P. Eh. Hovsepian, Lubricated sliding wear mechanism of chromium-doped graphite-like carbon coating, Tribology International, 77 (2014) 186–195

[13] E. A. Gulbransen, K. F. Andrew, F. A. Brassart, Studies On The High Temperature Oxidation Of Molybdenum, Tungsten, Niobium, Tantalum, Titanium, And Zirconium, Project Number: ARG-D-I96, Westinghouse Electric Corporation Research Laboratories, Pittsburgh, Pennsylvania 15235, April 18, 1967

[14] E. Lassner, W.D. Schubert, Tungsten: Properties, Chemistry, Technology of the Elements, Alloys, and Chemical Compounds, Springer Science & Business Media, 31 Jan 1999, Chapter 3, page 86

[15] M. L. Frauwallner, F. López-Linares, J. Lara-Romero, C. E Scott., V. Ali, E. Hernández, P. Pereira-Almao, Toluene hydrogenation at low temperature using a molybdenum carbide catalyst, Applied Catalysis A: General, 394 (2011) 62–70

[16] X. Chen, Z. Peng, Z. Fu, S. Wu, W. Yue, C. Wang, Microstructural, mechanical and tribological properties of tungsten-gradually doped diamond-like carbon films with functionally graded interlayers, Surface & Coatings Technology, 205 (2011) 3631–3638

[17] J. Chen, D. Lu, W. Zhang, F. Xie, J. Zhou, L. Gong, X. Liu, S. Deng, N. Xu, Synthesis and Raman spectroscopic study of W20O58 nanowires, J. Phys. D: Appl. Phys., 41 (2008) 115305

[18] D. Y. Lu, J. Chen, J. Zhou, S. Z. Deng, N. S. Xu, J. B. Xu, Raman spectroscopic study of oxidation and phase transition in W18O49 nanowires, J. Raman Spectrosc., 38 (2007) 176–180

[19] H. Knozinger, H. Jeziorowskl, Raman Spectra of Molybdenum Oxide Supported on the Surface of Aluminas, The Journal of Physical Chemistry, 82 (1978) 18

[20] M. Dieterle, G. Mestl, Raman spectroscopy of molybdenum oxides Part II. Resonance Raman spectroscopic characterization of the molybdenum oxides Mo4O11 and MoO2, Phys. Chem. Chem. Phys., 4 (2002) 822–826

[21] M. Dieterle, G. Mestl, J. Jäger, Y. Uchida, H. Hibst, R. Schlögl, Mixed molybdenum oxide based partial oxidation catalyst 2. Combined X-ray diffraction, electron microscopy and Raman investigation of the phase stability of (MoVW)5O14-type oxides, Journal of Molecular Catalysis A: Chemical, 174 (1-2) (2001) 169-185

[22] R. K. Sharma, G. B. Reddy, Influence of O2 − plasma ambience and growth temperature on the oxidation of Mo-metal and volatilization of oxides, AIP Advances, 3 (2013) 092112

[23] S. J. Oh, D.C. Cook, H.E. Townsend, Characterization of Iron Oxides Commonly Formed as Corrosion Products on Steel, Hyperfine Interactions, 112 (1-4) (1998) 59-66

[24] P.M. Sousa, A.J. Silvestre, N. Popovici, O. Conde, Morphological and structural characterization of CrO2/Cr2O3 films grown by Laser-CVD, Applied Surface Science, 247 (2005) 423–42

[25] J.E. Maslar, W.S. Hurst, W.J. Bowers Jr., J.H. Hendricks, M.I. Aquino, I. Levin, In situ Raman spectroscopic investigation of chromium surfaces under hydrothermal condition, Applied Surface Science, 180 (2001) 102-118

[26] Y. Zhu, L. Wang, W. Yao, L. Cao, The interface diffusion and reaction between Cr layer and diamond particle during metallization, Applied Surface Science, 171 (2001) 143-150

[27] A. P. Ehiasarian, J. G. Wen, and I. Petrov, Interface microstructure engineering by high power impulse magnetron sputtering for the enhancement of adhesion, J. Appl. Phys. 101 (2007) 054301

Table 1: Raman peaks of the metal carbides and metal oxides present in Mo−W−C coating after heat-treated to 400°C and 500°C

Raman peaks assigned at 400°C	Raman peaks (this work)	Raman peaks (literature)
Mo_2C	~ 342 cm^{-1} with a width of ~ 239 cm^{-1}	~ 334 cm^{-1} [15]
WC	~ 943 cm^{-1} with a width of ~ 76 cm^{-1}	~ 960 cm^{-1} [16]
Raman peaks assigned at 500°C	**Raman peaks (this work)**	**Raman peaks (literature)**
WO_3	~ 320 cm^{-1} with a width of ~ 213 cm^{-1}	~ 326 cm^{-1} [17]
$W_{18}O_{49}$		~ 100−400 cm^{-1} [18]
$W_{20}O_{58}$		~ 319 cm^{-1} [17]
Mo_2C	~ 462 cm^{-1} with a width of ~ 64 cm^{-1}	~ 470 cm^{-1} [15]
MoO_3		~ 474 cm^{-1} [19]
Mo_4O_{11}		~ 452 cm^{-1} [20]
$W_{20}O_{58}$		~ 463 cm^{-1} [19]
WO_3	~ 707 cm^{-1} with a width of ~ 112 cm^{-1}	~ 717 cm^{-1} [17]
$W_{18}O_{49}$		~ 600−800 cm^{-1} [18]
$W_{20}O_{58}$		~ 700 cm^{-1} [17]
Mo_2C	~ 817 cm^{-1} with a width of ~ 81 cm^{-1}	~ 819 cm^{-1} [15]
MoO_3		~ 820 cm^{-1} [19]
WO_3		~ 717 cm^{-1} [17]
WC	~ 944 cm^{-1} with a width of ~ 119 cm^{-1}	~ 960 cm^{-1} [16]
Mo_4O_{11}		~ 907 cm^{-1} and ~ 985 cm^{-1} [20]
Mo_5O_{14}		~ 902 cm^{-1} [21]
Mo_8O_{23}		~ 902 cm^{-1} and ~ 958 cm^{-1} [22]

Table 2: Raman peaks of the metal oxides present in Mo−W−C coating after heat-treated to 600°C

Raman peaks assigned at 600°C	Raman peaks (this work)	Raman peaks (literature)
WO_3	~ 99 cm^{-1} with a width of ~ 29.5 cm^{-1}	~ 95 cm^{-1} [17]
WO_3	~ 140 cm^{-1} with a width of ~ 27 cm^{-1}	~ 134 cm^{-1} [17]
$W_{18}O_{49}$		~ 100−400 cm^{-1} [18]
WO_3	~ 274 cm^{-1} with a width of ~ 34 cm^{-1}	~ 273 cm^{-1} [17]
$W_{18}O_{49}$		~ 100−400 cm^{-1} [18]
WO_3	~ 353 cm^{-1} with a width of ~ 73 cm^{-1}	~ 348 cm^{-1} [17]
MoO_3		~ 337 cm^{-1} and ~ 367 cm^{-1} [19]
Mo_4O_{11}		~ 340 cm^{-1} [20]
WO_3	~ 704 cm^{-1} with a width of ~ 77 cm^{-1}	~ 717 cm^{-1} [17]
$W_{18}O_{49}$		~ 600−800 cm^{-1} [18]
$W_{20}O_{58}$		~ 700 cm^{-1} [17]
Mo_4O_{11}	~ 789 cm^{-1} with a width of ~ 29 cm^{-1}	~ 790 cm^{-1} [20]
MoO_3	~ 842 cm^{-1} with a width of ~ 74 cm^{-1}	~ 820 cm^{-1} [19]
Mo_4O_{11}		~ 843 cm^{-1} [20]
Mo_5O_{14}		~ 845 cm^{-1} and ~ 860 cm^{-1} [21]
Mo_8O_{23}	~ 958 cm^{-1} with a width of ~ 52 cm^{-1}	~ 958 cm^{-1} [22]
WC		~ 960 cm^{-1} [16]

Table 3: Raman peaks of the metal oxides present in Mo−W−C coating after heat-treated to 700°C

Raman peaks assigned at 700°C	Raman peaks (this work)	Raman peaks (literature)
WO_3	~ 99 cm^{-1} with a width of ~ 27 cm^{-1}	~ 95 cm^{-1} [17]
WO_3	~ 138 cm^{-1} with a width of ~ 23.5 cm^{-1}	~ 134 cm^{-1} [17]
$W_{18}O_{49}$		~ 100−400 cm^{-1} [18]
WO_3	~ 271 cm^{-1} with a width of ~ 23.5 cm^{-1}	~ 273 cm^{-1} [17]
$W_{18}O_{49}$		~ 100−400 cm^{-1} [18]
WO_3	~ 345 cm^{-1} with a width of ~ 96 cm^{-1}	~ 348 cm^{-1} [17]
MoO_3		~ 337 cm^{-1} and ~ 367 cm^{-1} [19]
Mo_4O_{11}		~ 340 cm^{-1} [20]
Fe_2O_3	~ 495 cm^{-1}	~ 497 cm^{-1} [23]
WO_3	~ 707.5 cm^{-1} with a width of ~ 46 cm^{-1}	~ 717 cm^{-1} [17]
$W_{18}O_{49}$		~ 600−800 cm^{-1} [18]
$W_{20}O_{58}$		~ 700 cm^{-1} [17]
CrO_2		~ 700 cm^{-1} [24]
MoO_3	~ 837 cm^{-1} with a width of ~ 90 cm^{-1}	~ 820 cm^{-1} [19]
Mo_4O_{11}		~ 835 cm^{-1} and ~ 843 cm^{-1} [20]
Mo_5O_{14}		~ 845 cm^{-1} and ~ 860 cm^{-1} [21]
Mo_8O_{23}	~ 950 cm^{-1} with a width of ~ 32 cm^{-1}	~ 958 cm^{-1} [22]
WC		~ 960 cm^{-1} [16]

Table 4: Raman peaks of the metal carbides and metal oxides present in Mo−W−C coating after heat-treated to 800°C

Raman peaks assigned at 800°C	Raman peaks (this work)	Raman peaks (literature)
WO_3	~ 93 cm^{-1}	~ 95 cm^{-1} [17]
WO_3	~ 135 cm^{-1}	~ 134 cm^{-1} [17]
$W_{18}O_{49}$		~ 100−400 cm^{-1} [18]
WO_3	~ 202 cm^{-1}	~ 205 cm^{-1} [17]
MoO_3		~ 199 cm^{-1} [19]
Mo_4O_{11}		~ 206 cm^{-1} [20]
$W_{20}O_{58}$	~ 360 cm^{-1}	~ 359 cm^{-1} [17]
MoO_3		~ 367 cm^{-1} [19]
MoO_2		~ 357 cm^{-1} [15]
Fe_2O_3	~ 497 cm^{-1}	~ 497 cm^{-1} [23]
MoO_2	~ 552 cm^{-1}	~ 566 cm^{-1} [15]
Mo_4O_{11}		~ 568 cm^{-1} [20]
Cr_2O_3		~ 554 cm^{-1} [24]
		~ 552 cm^{-1} [25]
Cr_2C	~ 688 cm^{-1}	~ 695 cm^{-1} [26]
WO_3	~ 729 cm^{-1}	~ 717 cm^{-1} [17]
MoO_2		~ 732 cm^{-1} [15]
Mo_5O_{14}		~ 720 cm^{-1} [21]
CrO_2		~ 700 cm^{-1} [24]
$W_{20}O_{58}$	~ 836 cm^{-1}	~ 830 cm^{-1} [17]
MoO_3		~ 820 cm^{-1} [19]
Mo_4O_{11}		~ 835 cm^{-1} and ~ 843 cm^{-1} [20]
Mo_8O_{23}	~ 945 cm^{-1}	~ 958 cm^{-1} [22]
WC		~ 960 cm^{-1} [16]
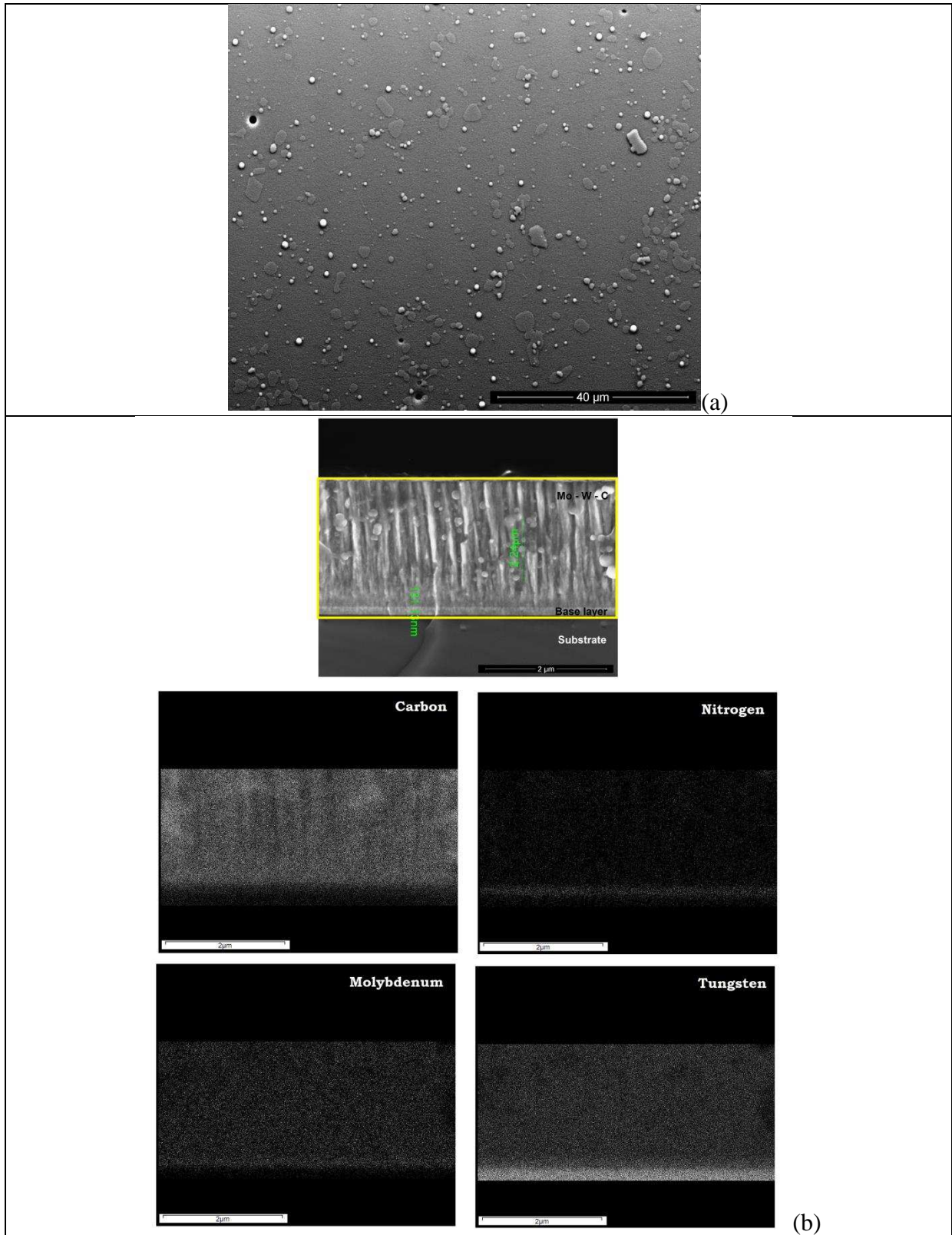
Figure 1: (a) Surface morphology and (b) X-ray mapping on the cross-section of as-deposited
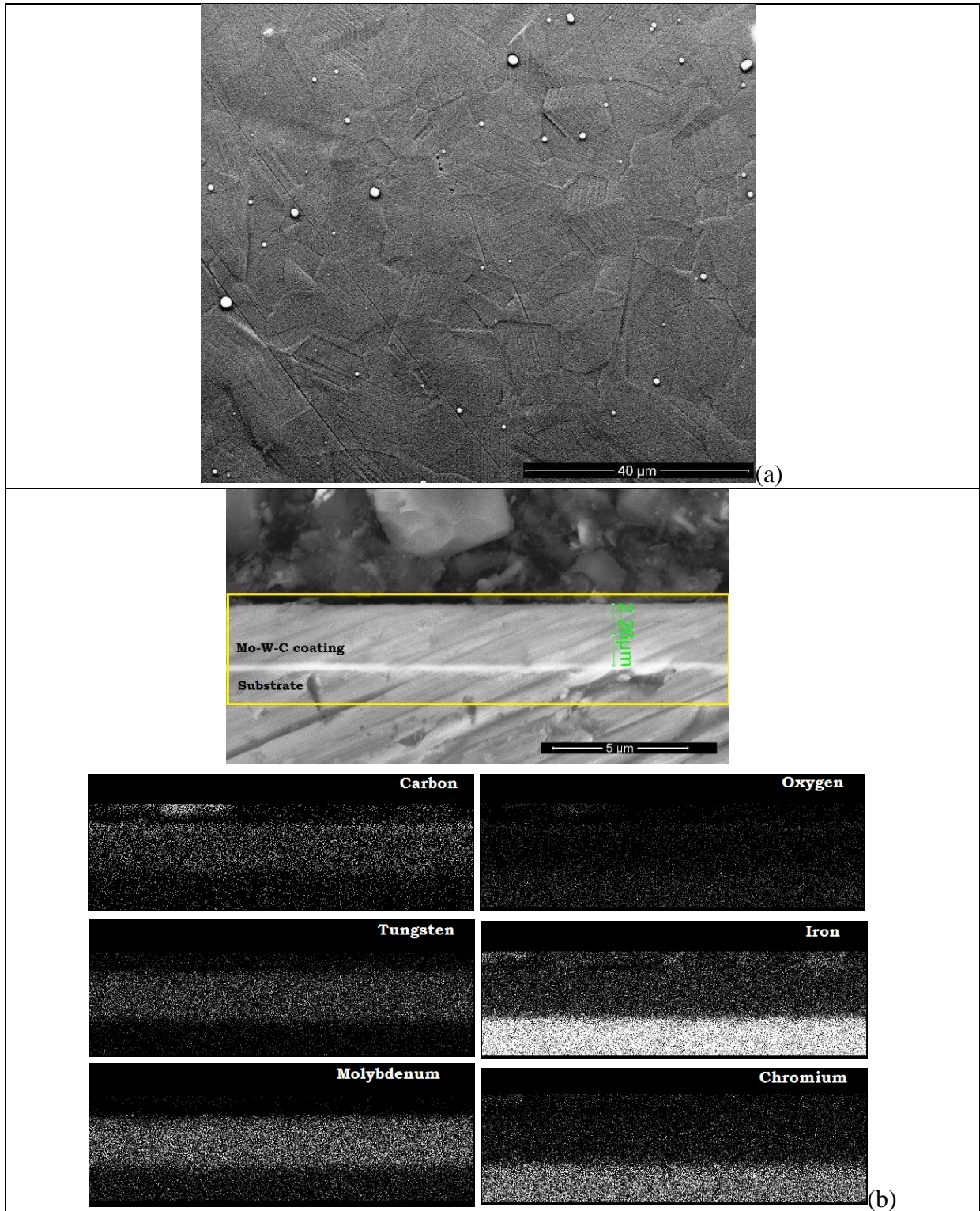
Mo−W−C coating

Figure 2: (a) Surface morphology and (b) X-ray mapping on the cross-section of Mo−W−C coated sample isothermally heated to 400°C
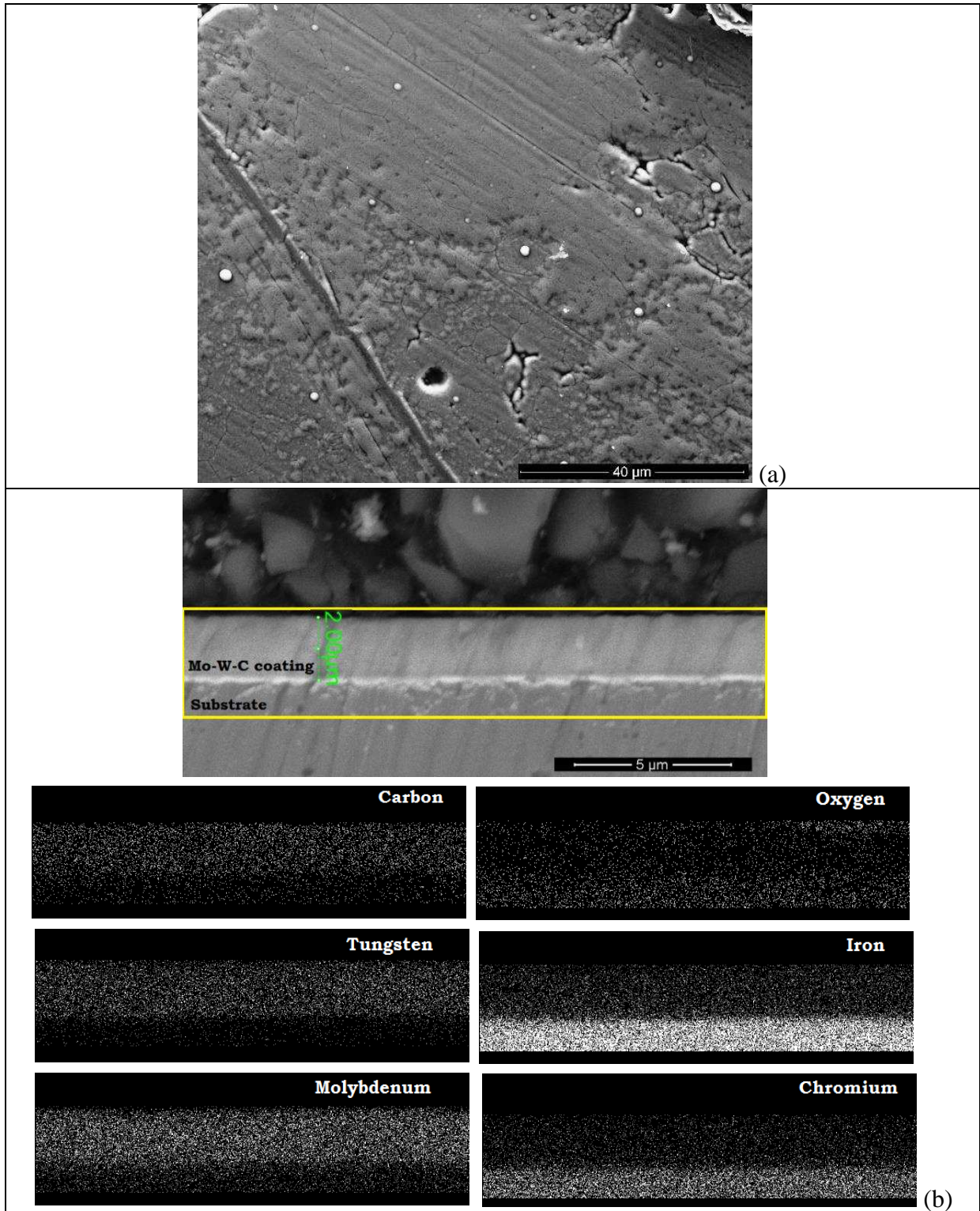
Figure 3: (a) Surface morphology and (b) X-ray mapping on the cross-section of Mo−W−C coated sample isothermally heated to 500°C
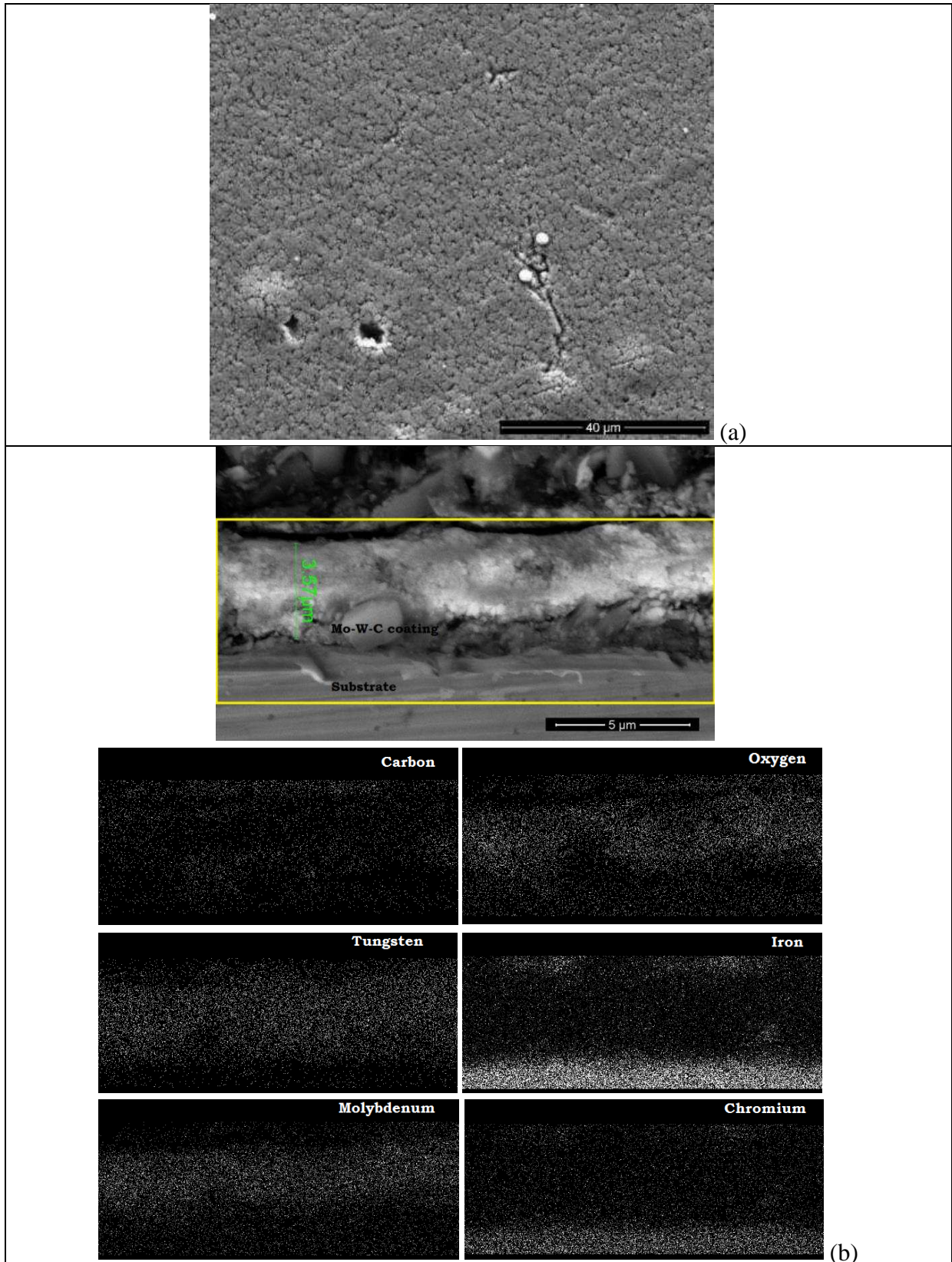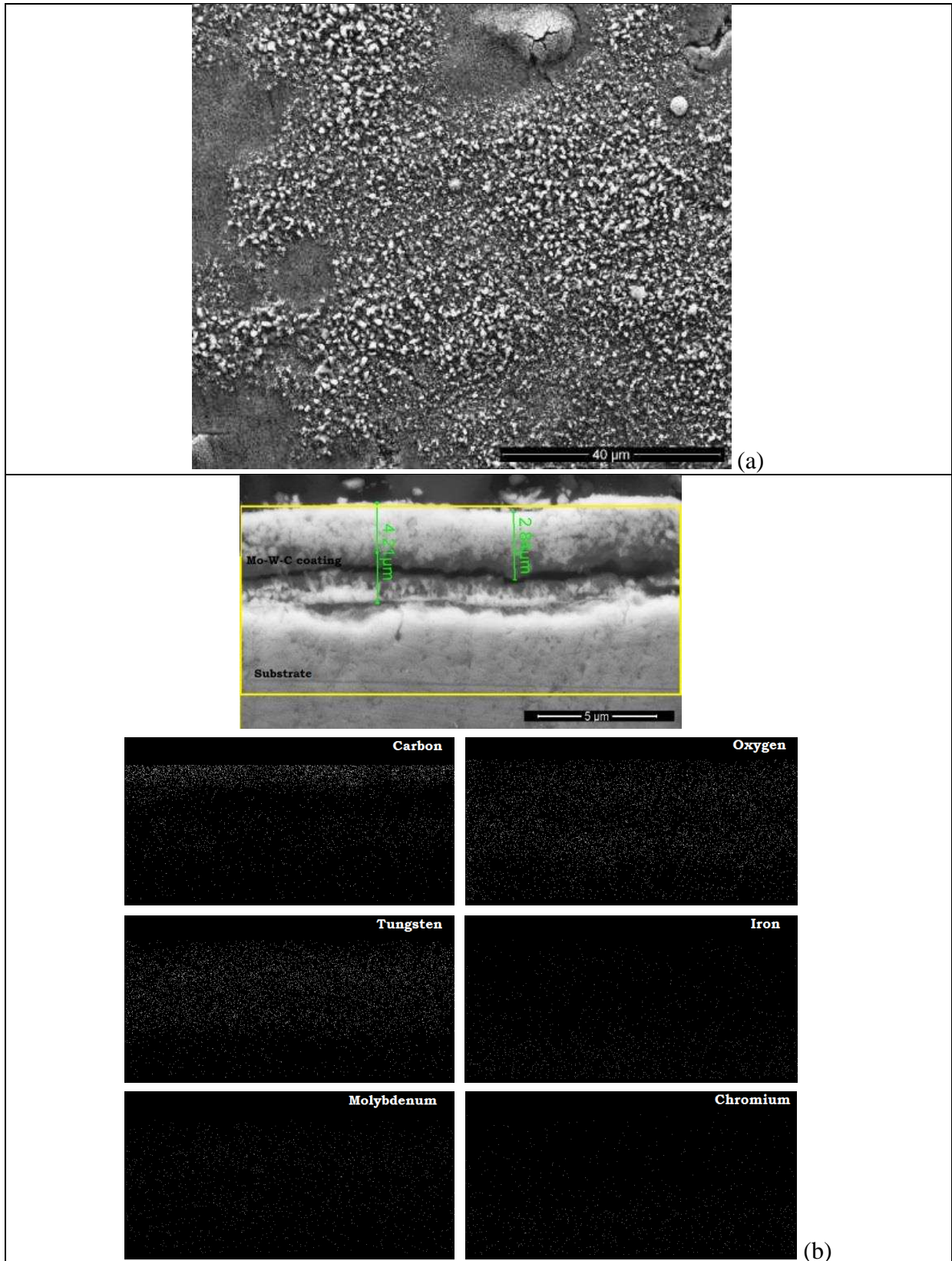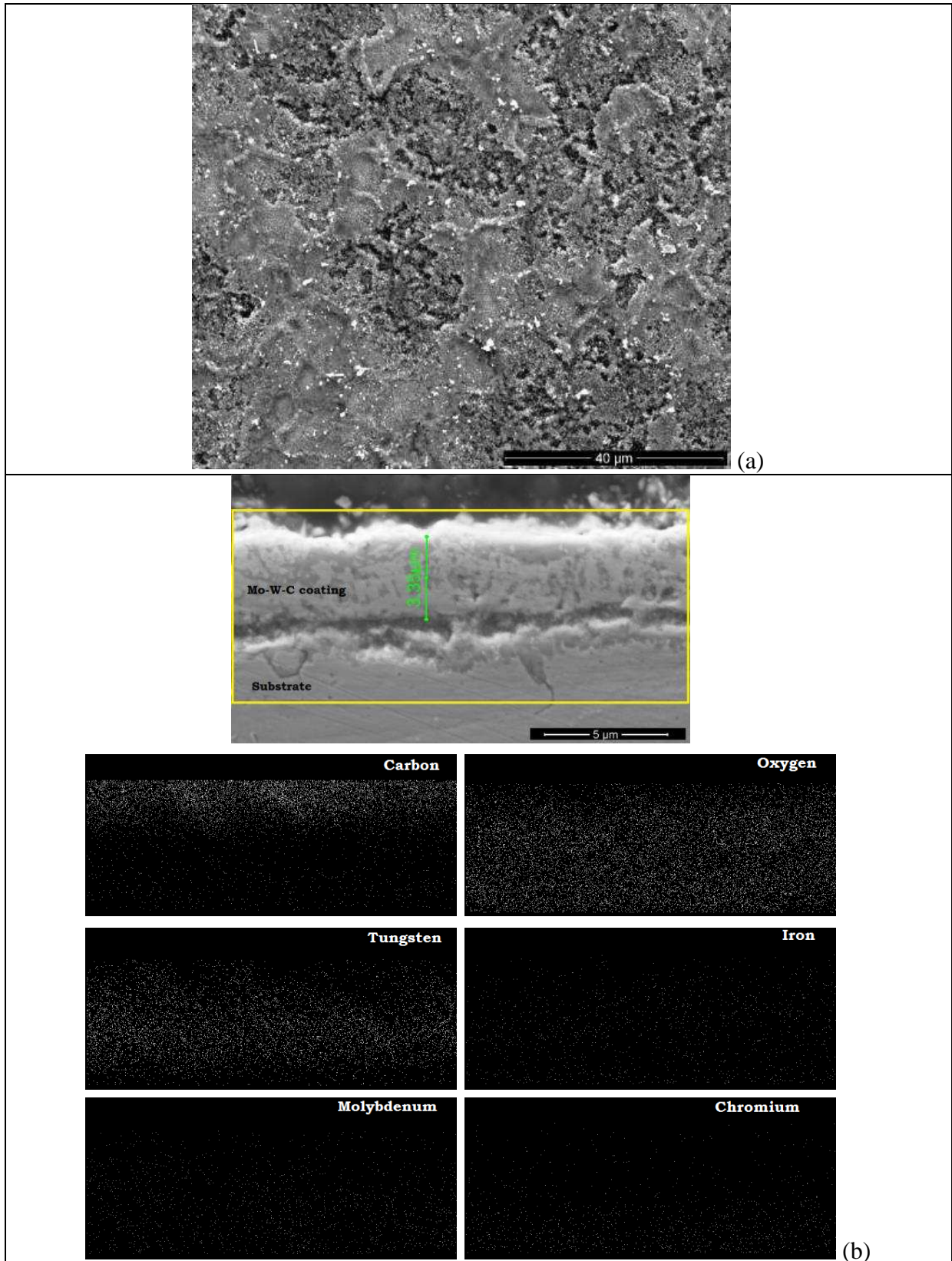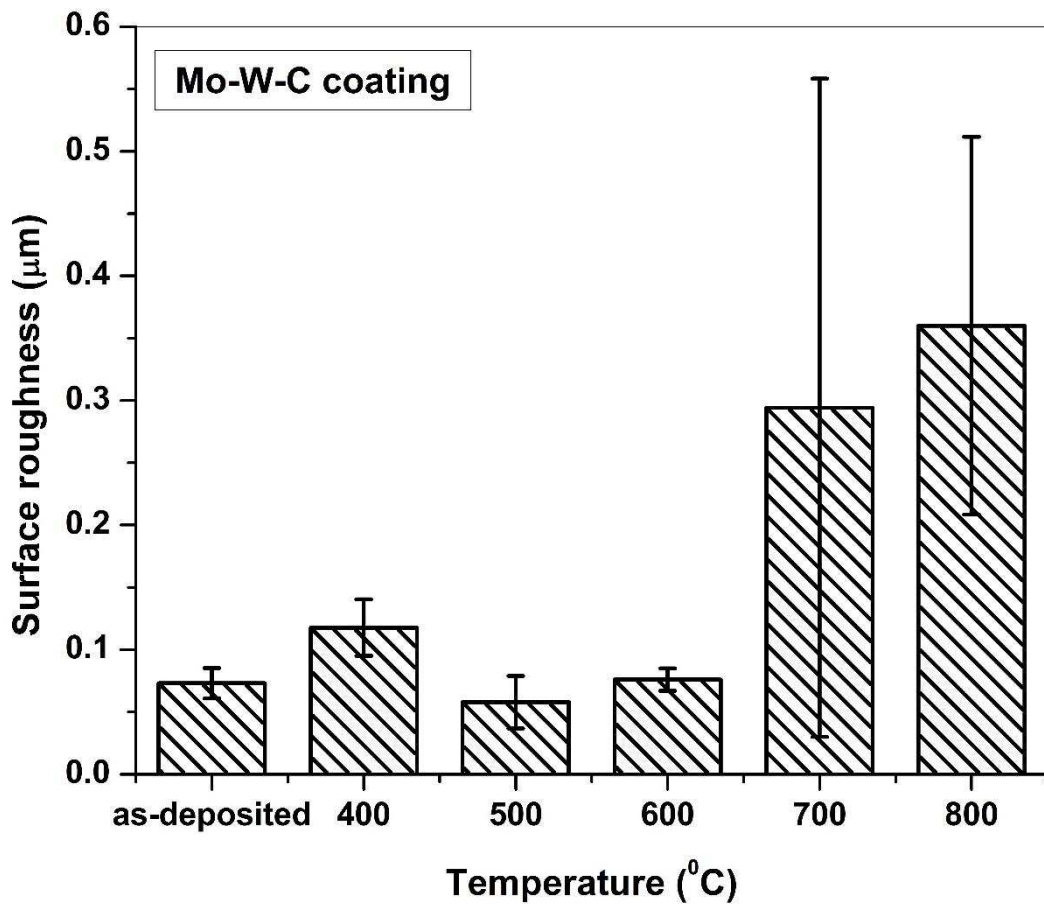
Figure 4: (a) Surface morphology and (b) X-ray mapping on the cross-section of Mo−W−C coated sample isothermally heated to 600°C

Figure 5: (a) Surface morphology and (b) X-ray mapping on the cross-section of Mo−W−C coated sample isothermally heated to 700°C

Figure 6: (a) Surface morphology and (b) X-ray mapping on the cross-section of Mo−W−C coated sample isothermally heated to 800°C

Figure 7: Average surface roughness of isothermally oxidised Mo−W−C coating
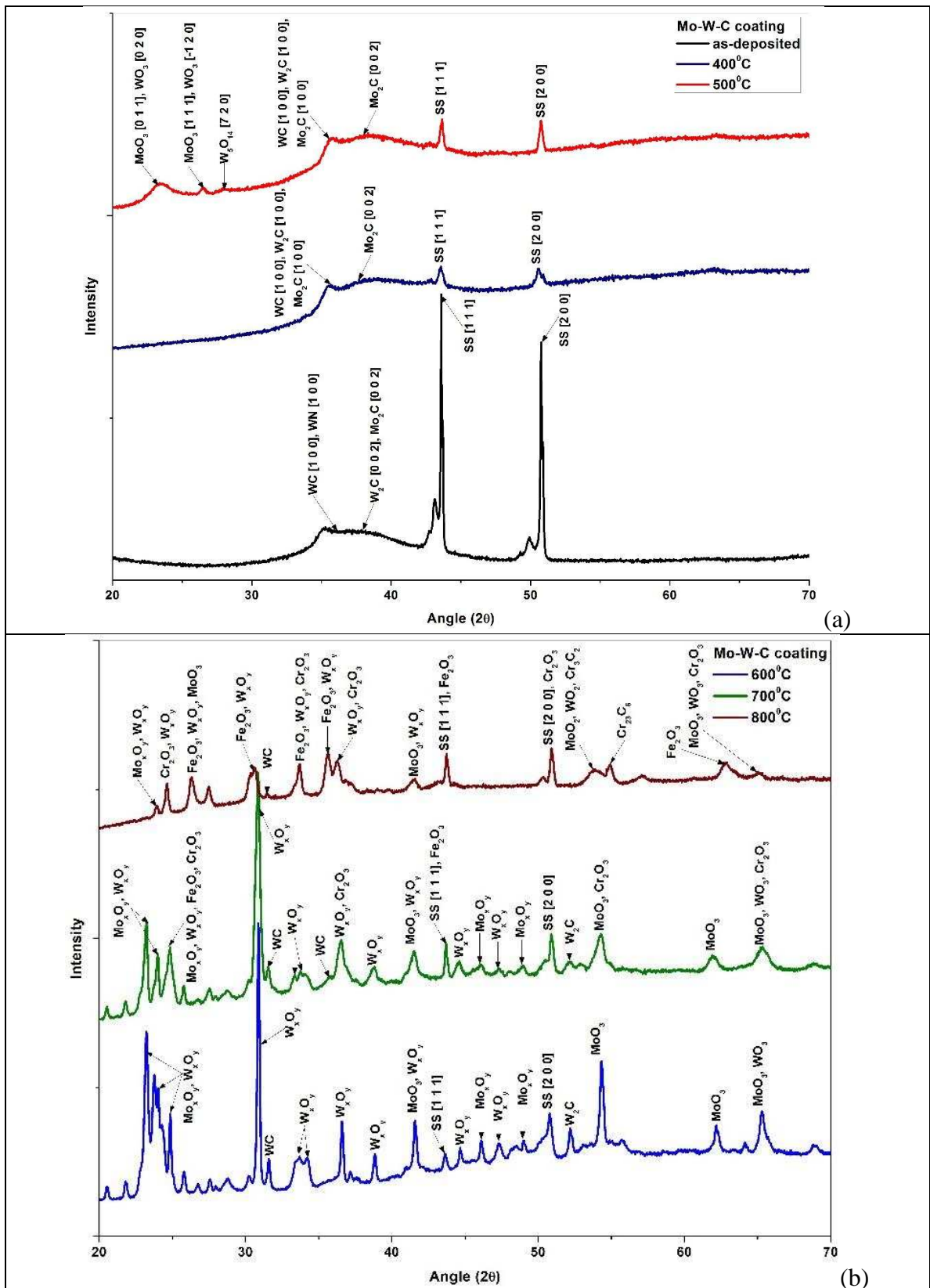
Figure 8: XRD patterns (using Bragg-Brentano geometry) of Mo−W−C coating (a) as-deposited − heat-treated at 500°C and (b) heat-treated at 600°C − 800°C
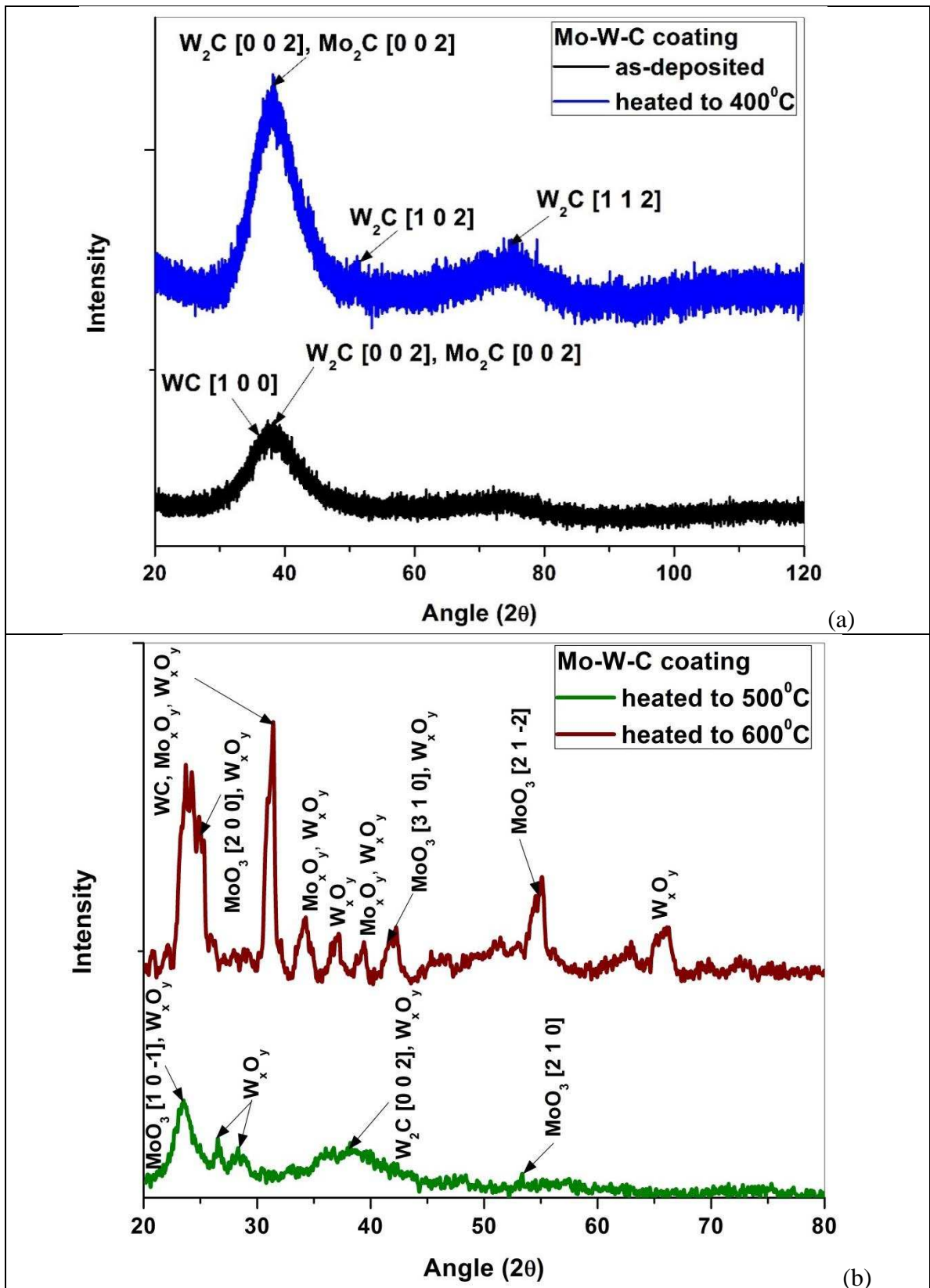
Figure 9: Glancing angle XRD patterns of Mo−W−C coating (a) as-deposited and heat-treated to 400°C, (b) heat-treated to 500°C and 600°C
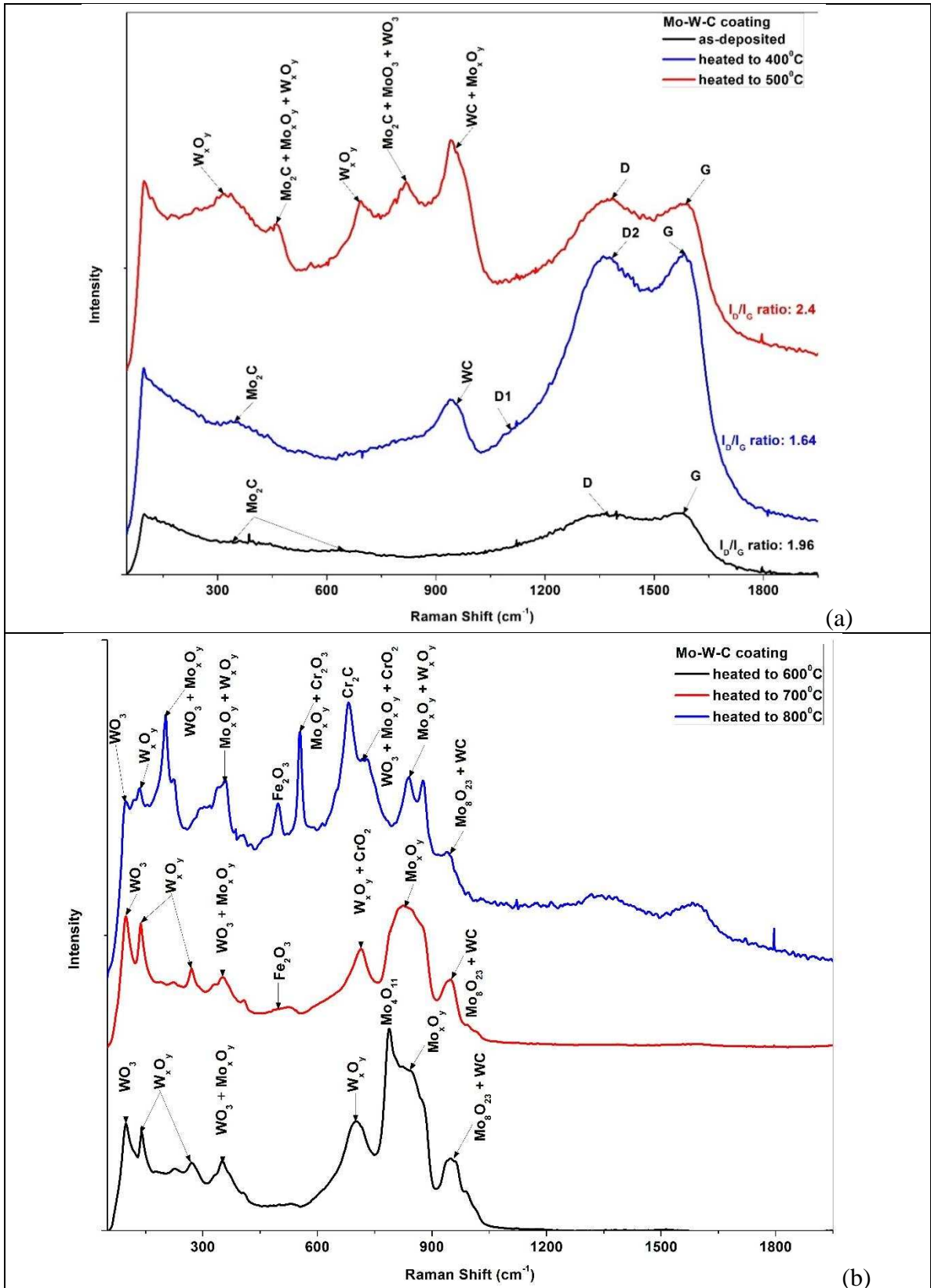
Figure 10: Raman spectra of Mo−W−C coating (a) as-deposited − heat-treated at 500°C and
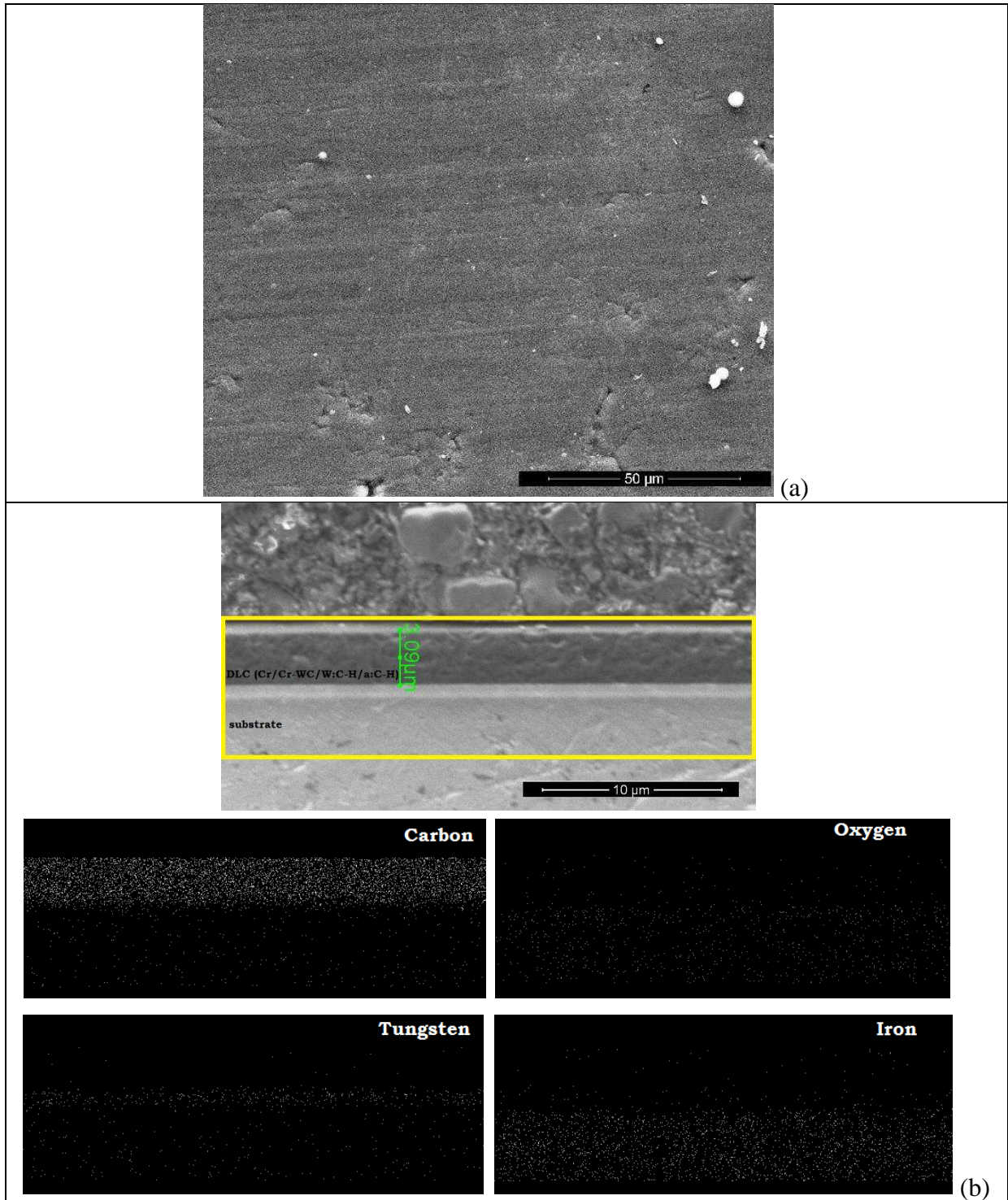
(b) heat-treated at 600°C − 800°C

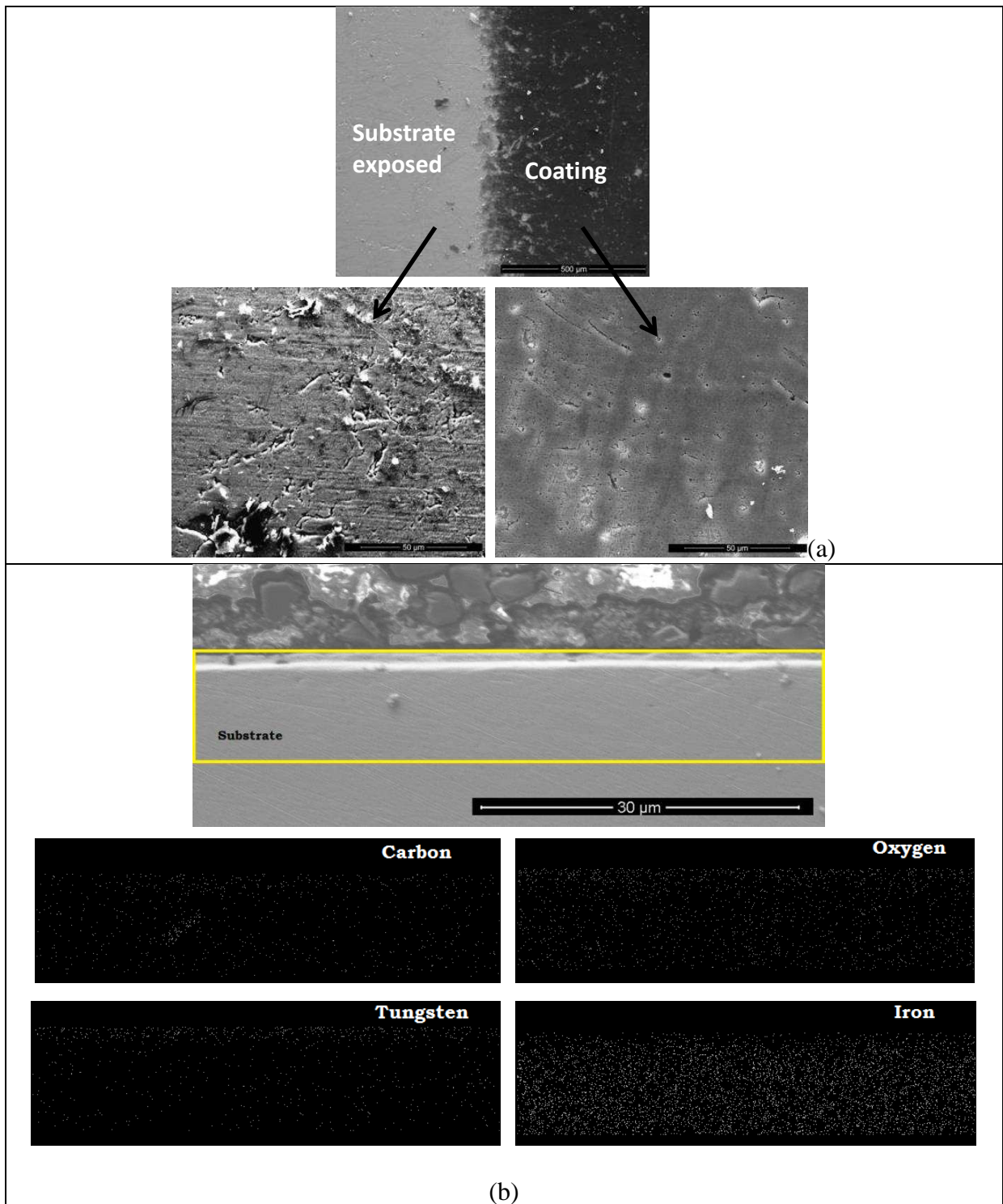Figure 11: (a) Surface morphology and (b) X-ray mapping on the cross-section of $\text{DLC}\left(\text{Cr}/\text{Cr}-\text{WC}/\text{W}:\text{C}-\text{H}/\text{a}:\text{C}-\text{H}\right)$ coated sample isothermally heated to 400°C
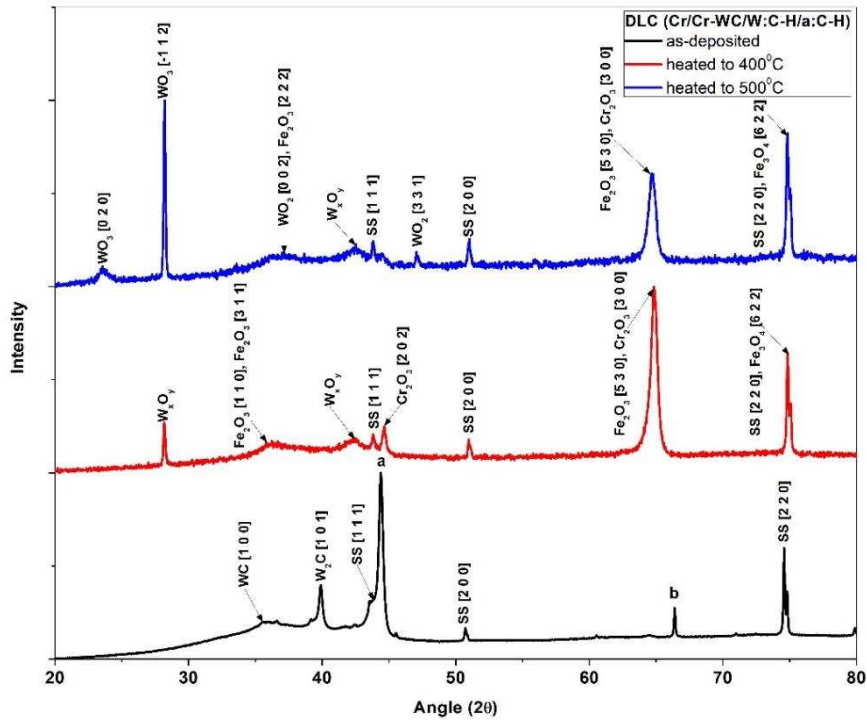
Figure 12: (a) Surface morphology and (b) X-ray mapping on the cross-section of

$\text{DLC}\left(\text{Cr}/\text{Cr}-\text{WC}/\text{W}:\text{C}-\text{H}/\text{a}:\text{C}-\text{H}\right)$ coated sample isothermally heated to 500°C

Figure 13: XRD patterns (using Bragg-Brentano geometry) of as-deposited and isothermally heat-treated $DLC\left(Cr / Cr - WC / W : C - H / a : C - H\right)$ coating
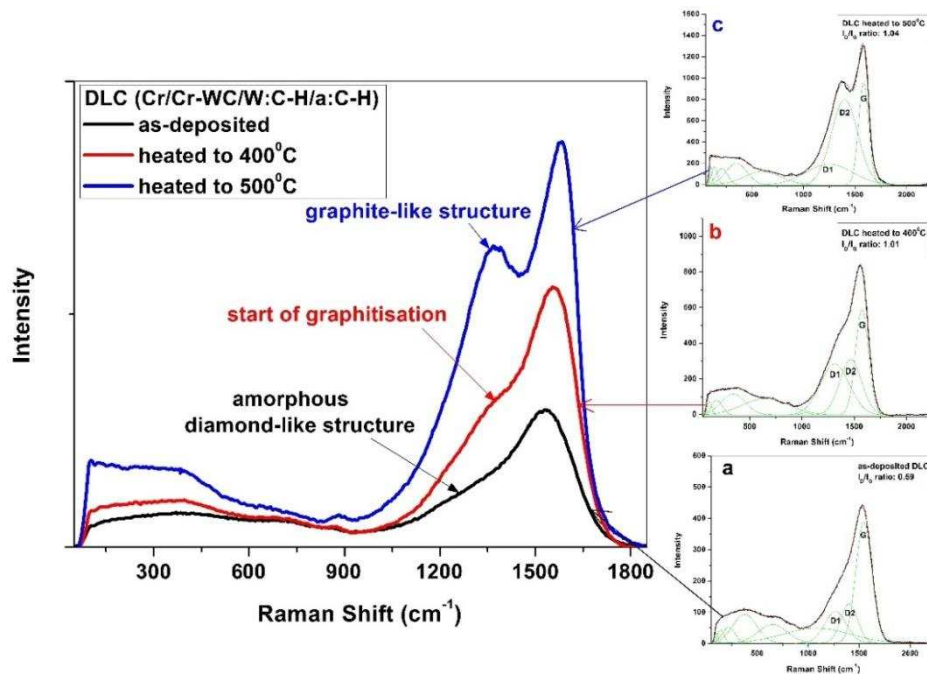

Figure 14: Raman spectra of as-deposited and isothermally heat-treated $DLC\left(Cr / Cr - WC / W : C - H / a : C - H\right)$ coating
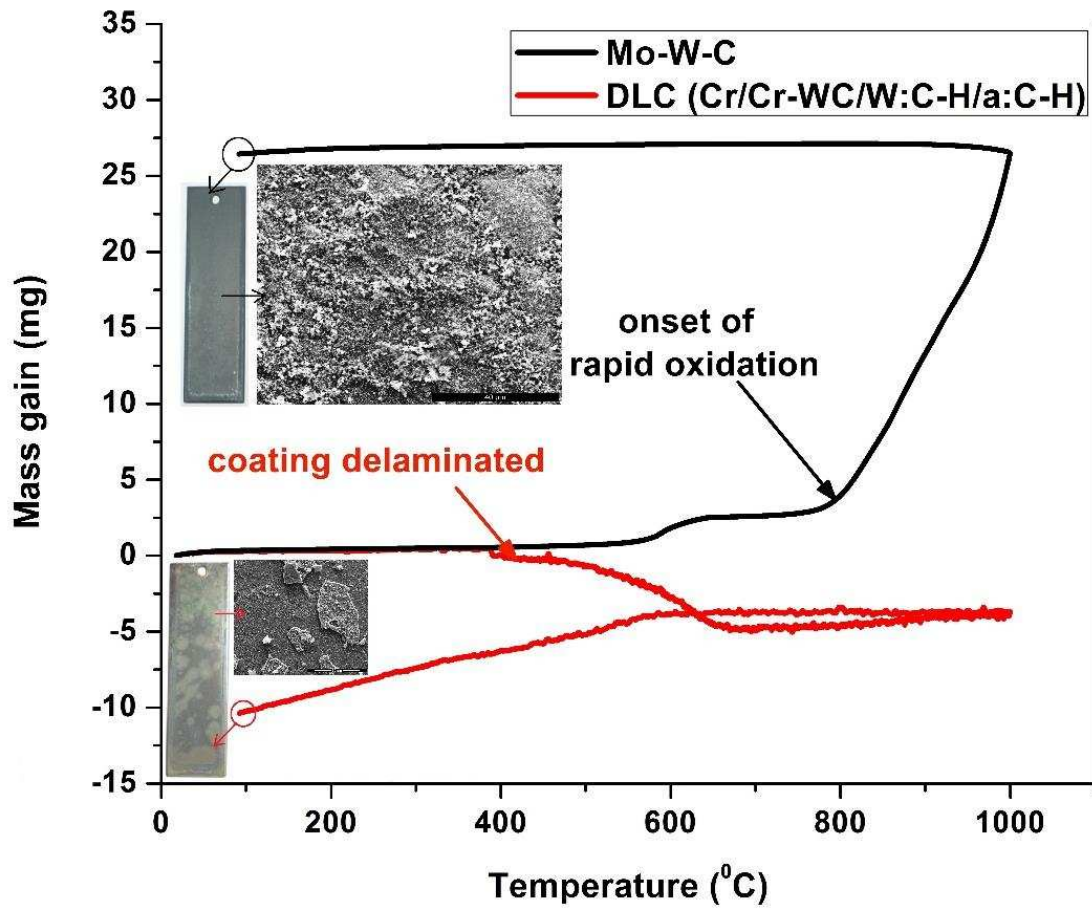
Figure 15: Thermo-gravimetric results obtained for Mo−W−C and $\mathrm{DLC}\left(\mathrm{Cr}/\mathrm{Cr}-\mathrm{WC}/\mathrm{W}:\mathrm{C}-\mathrm{H}/\mathrm{a}:\mathrm{C}-\mathrm{H}\right)$ coatings